OXFORD

Human Molecular Genetics, 2017, Vol. 26, No. 22 4465–4480

doi: 10.1093/hmg/ddx334
Advance Access Publication Date: 26 August 2017
Original Article

ORIGINAL ARTICLE

The integrity and organization of the human AIPL1 functional domains is critical for its role as a HSP90-dependent co-chaperone for rod PDE6

Almudena Sacristan-Reviriego[1], James Bellingham[1], Chrisostomos Prodromou[2], Annika N. Boehm[3], Annette Aichem[3], Neruban Kumaran[1], James Bainbridge[1], Michel Michaelides[1] and Jacqueline van der Spuy[1,*]

[1]UCL Institute of Ophthalmology, London EC1V 9EL, UK, [2]Genome Damage and Stability Centre, University of Sussex, Brighton, East Sussex BN1 9RQ, UK and [3]Biotechnology Institute Thurgau, University of Konstanz, Kreuzlingen, Switzerland

*To whom correspondence should be addressed at: UCL Institute of Ophthalmology, 11–43 Bath Street, London EC1V 9EL, UK. Tel: +44 2076084066; Email: j.spuy@ucl.ac.uk

Abstract

Biallelic mutations in the photoreceptor-expressed aryl hydrocarbon receptor interacting protein-like 1 (AIPL1) are associated with autosomal recessive Leber congenital amaurosis (LCA), the most severe form of inherited retinopathy in early childhood. AIPL1 functions as a photoreceptor-specific co-chaperone that interacts with the molecular chaperone HSP90 to facilitate the stable assembly of the retinal cyclic GMP (cGMP) phosphodiesterase (PDE6) holoenzyme. In this study, we characterized the functional deficits of *AIPL1* variations, some of which induce aberrant pre-mRNA *AIPL1* splicing leading to the production of alternative AIPL1 isoforms. We investigated the ability of the AIPL1 variants to mediate an interaction with HSP90 and modulate the rod cGMP PDE6 stability and activity. Our data revealed that both the FK506 binding protein (FKBP)-like domain and the tetratricopeptide repeat (TPR) domain of AIPL1 are required for interaction with HSP90. We further demonstrate that AIPL1 significantly modulates the catalytic activity of heterologously expressed rod PDE6. Although the N-terminal FKBP-like domain of AIPL1 binds the farnesylated PDE6α subunit through direct interaction with the farnesyl moiety, mutations compromising the integrity of the C-terminal TPR domain of AIPL1 also failed to modulate PDE6 activity efficiently. These AIPL1 variants moreover failed to promote the HSP90-dependent stabilization of the PDE6α subunit in the cytosol. In summary, we have successfully validated the disease-causing status of the *AIPL1* variations *in vitro*. Our findings provide insight into the mechanism underlying the co-chaperone role of AIPL1 and will be critical for ensuring an early and effective diagnosis of AIPL1 LCA patients.

Introduction

Leber congenital amaurosis (LCA) is the most rapid and severe inherited retinal degeneration that causes visual impairment in childhood (1). Typically inherited in an autosomal recessive manner, LCA is characterized by marked reduction or complete loss of both rod and cone photoreceptor responses within the first few years of life (2). To date, at least 25 genes have been

Received: June 29, 2017. **Revised:** August 14, 2017. **Accepted:** August 15, 2017

associated with LCA (RetNet; https://sph.uth.edu/retnet), including *AIPL1*, a gene comprised of six exons coding for the aryl hydrocarbon receptor interacting protein-like 1 (3). *AIPL1* mutations are estimated to account for 5–10% of LCA cases (RetNet) resulting in one of the most clinically severe forms of the disease (LCA type 4) (OMIM AIPL1; #604393) (4,5,6).

The 384 amino acid protein AIPL1, whose expression is limited to the retina and the pineal gland, shares 50% sequence identity with the ubiquitously expressed aryl hydrocarbon receptor interacting protein AIP (3,7). Functionally, AIPL1 is similar to FK506 binding protein (FKBP)51, FKBP52 and AIP, all of which are members of a group of co-chaperones that interact with the molecular chaperone HSP90 via a conserved C-terminal tetratricopeptide repeat (TPR) domain (8–10). The AIPL1 TPR domain consists of three TPR motifs, which are highly degenerate 34 amino acid repeats (11,12). HSP90, typically the most abundant cytoplasmic adenosine triphosphate (ATP)-dependent molecular chaperone in vertebrate cells, is a dynamic dimer that acts in complex with co-chaperones on native-like protein substrates called clients, serving a vital role in cellular signalling by regulating client folding, activity and stability (13). Each HSP90 monomer consists of three functionally distinct domains: a N-terminal domain (NTD) that confers nucleotide binding, a middle domain (MD) necessary for ATPase activity and a C-terminal domain (CTD) responsible for constitutive dimerization (14). A highly conserved IEEVD or MEEVD motif located at the very C-terminus of HSP70 and HSP90, respectively, is the primary interaction site for the TPR domain-containing co-chaperones, including AIPL1 (10,15–18). However, the affinity and specificity of the interaction of the TPR domain co-chaperones with HSP90 may involve charged and hydrophobic residues upstream of the HSP90 MEEVD sequence as well as contacts outside of the TPR motifs (19–22). In addition, human AIPL1 harbours a unique primate-specific unstructured C-terminal proline-rich domain (PRD), which has been reported to influence the association with HSP90 in an inhibitory manner or have no effect thereupon (23,24).

Several *in vivo* and *in vitro* studies have established a link between AIPL1 and the cyclic nucleotide phosphodiesterase of the sixth family (PDE6), a holoenzyme that catalyses the hydrolysis of cyclic GMP (cGMP) upon light stimulation in photoreceptor cells. *Aipl1* knockout and hypomorphic murine models revealed that in the absence of AIPL1, the PDE6 subunits are misassembled and rapidly targeted for proteasomal degradation, leading to the absence of a response to light stimuli and triggering rapid degeneration of the rod and cone photoreceptors (25–29). Recently, it was reported that AIPL1 is required to reconstitute the catalytic activity of the heterologously expressed cone PDE6 (30). The N-terminal FKBP-like domain of AIPL1, which lacks peptidylprolyl isomerase activity (22) directly binds a farnesyl or geranylgeranyl moiety *in vitro* (24,31–33) and is therefore proposed to mediate the interaction with the farnesylated rod PDE6α subunit and with the geranylgeranylated rod PDE6β and cone PDE6α' subunits. Finally, PDE6 has been identified as an HSP90 client as inhibition of HSP90 *in vivo* in the retina led to a posttranslational reduction in PDE6 levels (34).

The *AIPL1* gene is highly polymorphic with more than 400 *AIPL1* variations annotated in the Exome Aggregation Consortium (ExAC) data set (exac.broadinstitute.org). We have recently reported that missense or intronic variations in *AIPL1* cause aberrant pre-mRNA splicing leading to the production of transcripts that could encode functionally deficient protein isoforms (35). Although *in silico* prediction tools are frequently used to ascertain the probable pathogenicity of genetic variations, only a handful have been experimentally validated and reported as pathogenic mutations (Human Gene Mutation Database; http://www.hgmd.org) (31,32,36–39). In this study, we investigated the functional impact of novel and uncharacterized *AIPL1* nonsense, missense and intronic variations to confirm their disease-causing status and gain insight into the role of AIPL1 as a HSP90 co-chaperone for PDE6. We investigated the interaction of the AIPL1 variants with HSP90 and their requirement for the stable expression and function of rod PDE6.

Results

AIPL1 variations investigated

In this study, we engineered LCA associated non-synonymous missense and nonsense variations as well as small insertions and duplications in the coding sequence of the *AIPL1* cDNA (Fig. 1A). The resultant amino acid changes are distributed throughout AIPL1 including the N-terminal FKBP-like domain and the C-terminal TPR domain (Fig. 1A and B). Intronic canonical splice site variations, small deletions spanning a canonical splice site and small coding insertions and duplications or missense variations in the first or last base of an exon immediately adjacent to a canonical splice site were all recently confirmed to induce aberrant splicing of the *AIPL1* gene (35) (Fig. 1C). We engineered the AIPL1 protein isoforms predicted to be translated from these alternative transcripts in the coding sequence of the *AIPL1* cDNA to investigate their impact on AIPL1 function (Fig. 1C and D). All of these *AIPL1* variations completely abolished native splice site recognition (35), except c.97_104dupGTGATCTT and c.98_99insTGATCTTG, where native splice site recognition led to the translation of the frameshift stopped products p.F35Lfs*2 and p.I34Dfs*10, respectively (Fig. 1A), whilst aberrant transcription lead to the production of p.V33Sfs*57 (Fig. 1C). The coding missense variations c.465G > T, c.642G > C and c.784G > A also completely abolished native splice site recognition leading to the complete loss of transcripts coding for p.Q155H, p.K214N and p.G262S, respectively, and the exclusive expression of alternative transcripts (35) (Fig. 1C). However, in addition to engineering the expected protein isoforms expressed as a result of alternative transcription (Fig. 1C), we also engineered c.642G > C (p.K214N) and c.784G > A (p.G262S) in the coding sequence of the *AIPL1* cDNA (Fig. 1A and B) to investigate their impact on AIPL1 function and confirm *AIPL1* missplicing as the underlying cause of disease in LCA patients harbouring these variations. We investigated the frequency of all the *AIPL1* variations investigated in this study in the current ExAC data set of 60 706 unrelated individuals (Supplementary Material, Table S1). Several of the variations investigated are not identified while the remainder are all very rare (allele frequency < 1/10 000), and none are observed in the homozygous state. *In silico* analysis of the missense variations reveals that all are predicted to be damaging, with the exception of c.465G > T (p.Q155H) and c.784G > A (p.G262S) which are predicted to be benign by at least one prediction programme.

Premature translation termination leads to AIPL1 misfolding and aggregation

We first investigated the expression and subcellular localization of the AIPL1 variants by western blotting and immunofluorescent confocal microscopy (Fig. 2). The myc tagged AIPL1 variants, p.L17P, p.G64R, p.C89R, p.V71F, p.Q163*, p.K214N and p.E282_283dup, were all similar to wild-type (w/t) AIPL1 in their expression (Fig. 2A and B) and subcellular distribution (Fig. 2C). Similarly, western blotting and immunofluorescence confocal

A

Genetic Change	Predicted Protein Change
c.50T>C	p.L17P
c.94C>T	p.R32*
c.97_104dupGTGATCTT	p.F35Lfs*2
c.98_99insTGATCTTG	p.I34Dfs*10
c.105_112dup	p.R38Lfs*6
c.190G>C	p.G64R
c.211G>T	p.V71F
c.216G>A	p.W72*
c.264G>A	p.W88*
c.265T>C	p.C89R
c.487C>T	p.Q163*
c.642G>C	p.K214N
c.784G>A	p.G262S
c.834G>A	p.W278*
c.844_849dup	p. E282_A283dup

C

Genetic Change	Protein Isoform Encoded by Alternative Transcript
c.97_104dupGTGATCTT	p.V33Sfs*57
c.98_99insTGATCTTG	p.V33Sfs*57
c.276+1G>A	p.V33_I92del, p.V33_Q155del, p. V156Efs*50
c.276+2T>C	p.V33_I92del, p.V33_Q155del, p.H93Afs*66
c.277-2A>G	p.H93_Q155del
c.465G>T	p.H93_Q155del, p.V148_Q155del
c.642G>C	p.V156_K214del, p.K214N_E215insVRGRWPG
c.784G>A	p.E215Afs*3, p.V249Afs*3
c.785-10_786del12	p.I263Afs*3, p.G262_A275del p.G262Efs*109

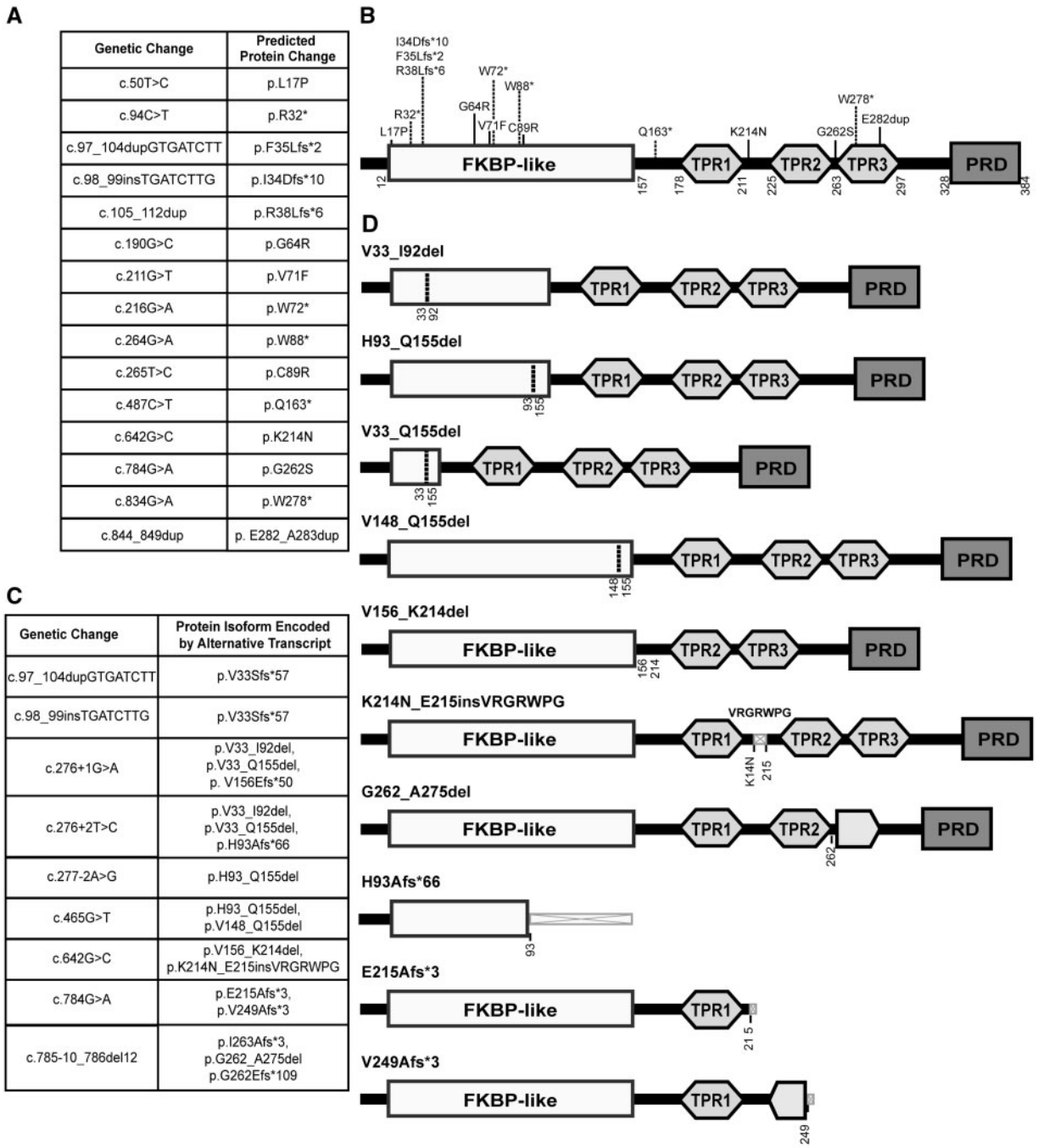

Figure 1. *AIPL1* variations investigated associated with LCA. (**A**) Non-synonymous missense and nonsense variations, small insertions and duplications in the coding sequence of *AIPL1* and their predicted changes in the AIPL1 amino acid sequence. (**B**) Schematic representation of the domain structure of AIPL1. The protein consists of an amino-terminal FKBP-like domain, a TPR domain that encompasses three consecutive TPR motifs and the primate-specific polyPRD. The diagram indicates which AIPL1 variants were analysed in this study. (**C**) Genetic variations in *AIPL1* coding and non-coding sequences that induce aberrant pre-mRNA splicing resulting in the indicated protein isoforms. (**D**) Schematic representation of AIPL1 protein isoforms encoded by alternative *AIPL1* transcripts including in-frame domain deletions as a result of in-phase exon skipping, frame-shift stop mutations and small insertions and deletions. Inclusion of non-native AIPL1 amino acid sequence induced by a frame-shift is shown as light grey crossed out boxes.

microscopy revealed that AIPL1 isoforms resulting from alternative transcription (p.V33_I92del, p.V33_Q155del, p.H93_Q155del, p.V148_Q155del, p.V156_K214del, p.K214_E215insVRGRWPG, p.V249Afs*3 and p.G262_A275del) were also comparable to w/t AIPL1 in their expression (Fig. 2D) and subcellular localization (Fig. 2E). However, the nonsense premature translation termination variants p.W72*, p.W88* and p.W278* (Fig. 2C), and the frameshift premature translation termination products p.H93Afs*66 and p.E215Afs*3 (Fig. 2E) formed intracellular inclusions that were visible by immunofluorescent confocal microscopy. Although p.W72* and p.W88* were detected by western blotting (Fig. 2B), p.W278* forms detergent insoluble intracellular aggregates that can be trapped on a filter (38) and thus did not resolve efficiently by denaturing SDS-PAGE (Fig. 2A).

Similarly, p.H93Afs*66 and p.E215Afs*3 formed intracellular aggregates of misfolded proteins (Fig. 2E) that were not resolved efficiently by denaturing SDS-PAGE (Fig. 2D). Interestingly, the nonsense premature translation termination variant p.Q163* (Fig. 2A, B and C) and the frameshift premature translation termination variant p.V249Afs*3 produced as a result of alternative splicing (Fig. 2D and E) were detected by western blotting but did not form intracellular aggregates in cells and were similar to w/t AIPL1 in their subcellular distribution. Finally, nonsense and frameshift stop mutations resulting in the large C-terminal truncation of AIPL1 (p.R32*, p.I34Dfs*10, p.F35Lfs*2 and p.R38Lfs*6) were not detected by western blotting or immunofluorescent confocal microscopy with an antibody directed against either the C-terminal AIPL1-specific epitope or the N-terminal myc tag due to their very small size (~3 kDa) (Fig. 2A and B) and were thus not investigated further. In summary, all the premature translation termination products detected in our assay, except p.Q163* and p.V249Afs*, formed intracellular protein inclusions. All the remaining AIPL1 variants were similar to w/t AIPL1.

Notably, the expression of all the AIPL1 variants investigated was driven from the same promoter under the same experimental conditions in cells leading to similar or elevated levels detected by western blotting compared with w/t AIPL1, with the exception of p.H93Afs*66, p.V249Afs*3 and p.W278* which were not resolved efficiently by SDS-PAGE. Yet, the formation of intracellular aggregates was evident only for p.W72*, p.W88*, p.H93Afs*66, p.E215Afs*3 and p.W278* but not p.Q163* and p.V249Afs*3 or any of the other variants investigated, suggesting that the formation of these aggregates occurs as a result of misfolding rather than due to protein overexpression. Interestingly, the c.834G > A substitution coding for p.W278* is located in the final exon of *AIPL1* and the resultant transcript may therefore escape nonsense-mediated mRNA decay (NMD) *in vivo* in photoreceptors, whilst the transcripts coding for all the other premature translation termination products are predicted to be subject to NMD due to the presence of premature termination codons. However, if these transcripts were to escape NMD *in vivo*, the resultant premature translation termination products would likely misfold leading to loss of function, except in the case of p.Q163* and p.V249Afs*3 which did not misfold in cells. Thus, p.Q163* and p.V249Afs*3 as well as all the AIPL1 variants that that did not misfold in intracellular inclusions were investigated further to determine their impact on AIPL1 function.

Nucleotide binding facilitates the interaction of AIPL1 with HSP90

AIPL1 can interact with the molecular chaperone HSP90, the conformational chaperone cycle of which is regulated by ATP binding and hydrolysis (14). The interaction of AIPL1 with HSP90 as a co-chaperone is poorly understood. We therefore investigated the nucleotide dependence of the interaction of AIPL1 with HSP90 using co-immunoprecipitation and quantitative ELISA (Fig. 3). Myc-AIPL1 and HA-HSP90 were reciprocally co-immunoprecipitated (Fig. 3A). Although HA-HSP90 was specifically co-immunoprecipitated by myc-AIPL1, a small amount of myc-AIPL1 was non-specifically detected in the absence of HA-HSP90. The co-immunoprecipitation of HA-HSP90 with myc-AIPL1 was enhanced by the addition of either ATP (5 mM) or adenosine diphosphate (ADP) (5 mM), with the addition of ATP having a greater effect than ADP (Fig. 3B). Conversely, the interaction was reduced by the addition of apyrase (Fig. 3C). These data suggest that AIPL1 preferentially associates with nucleotide-bound HSP90. Quantitative ELISA corroborated these findings. The interaction of myc-AIPL1 with untagged purified HSP90α was significantly enhanced by the addition of 5 mM ATP or ADP, with steady-state levels attained more rapidly in the presence of ATP than ADP (Fig. 3D), and the addition of apyrase significantly reducing the interaction (Fig. 3E). HSP990, a specific HSP90 inhibitor, also reduced the interaction of myc-AIPL1 with HSP90α particularly in the absence of added nucleotide (Fig. 3F). Similar results were obtained with AIPL1 and HSP90β (data not shown). Altogether, the results confirm that AIPL1 interacts preferentially with nucleotide-bound HSP90, particularly ATP-bound HSP90.

The interaction of AIPL1 with HSP90 is reduced by mutations in the TPR and FKBP-like domains

The interaction of HSP90 with the AIPL1 variants was investigated by directed yeast two-hybrid (Y2H) analysis and by quantitative ELISA, and compared with that of w/t AIPL1 to assess any deficits in HSP90 interaction (Figs 4 and 5). The interaction with HSP90 lacking the C-terminal MEEVD motif was also investigated, as this motif is important in mediating the interaction of the TPR domain with HSP90 (10). In the Y2H assays, yeast co-transformed with the positive control plasmids, pSos-MAFB and pMyr-MAFB, grew on selective media at both the permissive (24°C) and restrictive (37°C) temperatures (Fig. 4A). The interaction of the Sos-MAFB and Myr-MAFB proteins localized hSos to the cell membrane via the myristoylation signal, thereby activating the Ras pathway and rescuing the temperature-sensitive phenotype of the cdc25H strain on selective media. Yeast co-transformed with empty pSos and empty pMyr, with empty pSos and pMyr-HSP90, or with empty pSos and pMyr-HSP90ΔMEEVD grew on selective media at the permissive temperature but did not rescue growth at 37°C and were therefore used as internal negative controls in the assay. In the directed Y2H assays of the AIPL1 variants from coding variations (Fig. 4A), w/t AIPL1 interacted with HSP90 and this interaction was reduced by deletion of the HSP90 C-terminal MEEVD, confirming that the MEEVD motif contributes to the binding of AIPL1 to HSP90. The premature stop mutant p.W278* did not induce growth at the restrictive temperature, as previously reported (10). No growth at the restrictive temperature was seen in yeast cells transformed with HSP90 and the AIPL1 variants p.L17P, p.C89R and p.E282_A283dup revealing a deficit in their ability to interact with HSP90. The AIPL1 variants p.G64R, p.V71F, p.K214N and p.G262S were able to interact with HSP90 in a TPR-dependent manner similar to w/t AIPL1 in the Y2H assay. It has previously been reported that p.G262S does not impact AIPL1 function (10,30,37,38). Similarly, p.K214N did not affect AIPL1 interaction with HSP90. However, both c.642G > C (p.K214N) and c.784G > A (p.G262S) abolish native *AIPL1* splicing leading to the production of alternative isoforms (35). Interestingly, the p.Q163* variant, which lacks the entire AIPL1 TPR domain, was able to rescue growth with both HSP90 and HSP90ΔMEEVD, suggesting non-specific transactivation by p.Q163* in the Y2H assay. Western blotting confirmed the expression of the AIPL1 variants in yeast cell lysates (Fig. 4B), with the exception of p.W278* which is trapped in detergent-insoluble inclusions in cells (Fig. 2D).

We performed a quantitative ELISA to quantify the interaction of the AIPL1 variants with full-length human HSP90α and HSP90β (Fig. 4C). The absorbance of each AIPL1 variant was

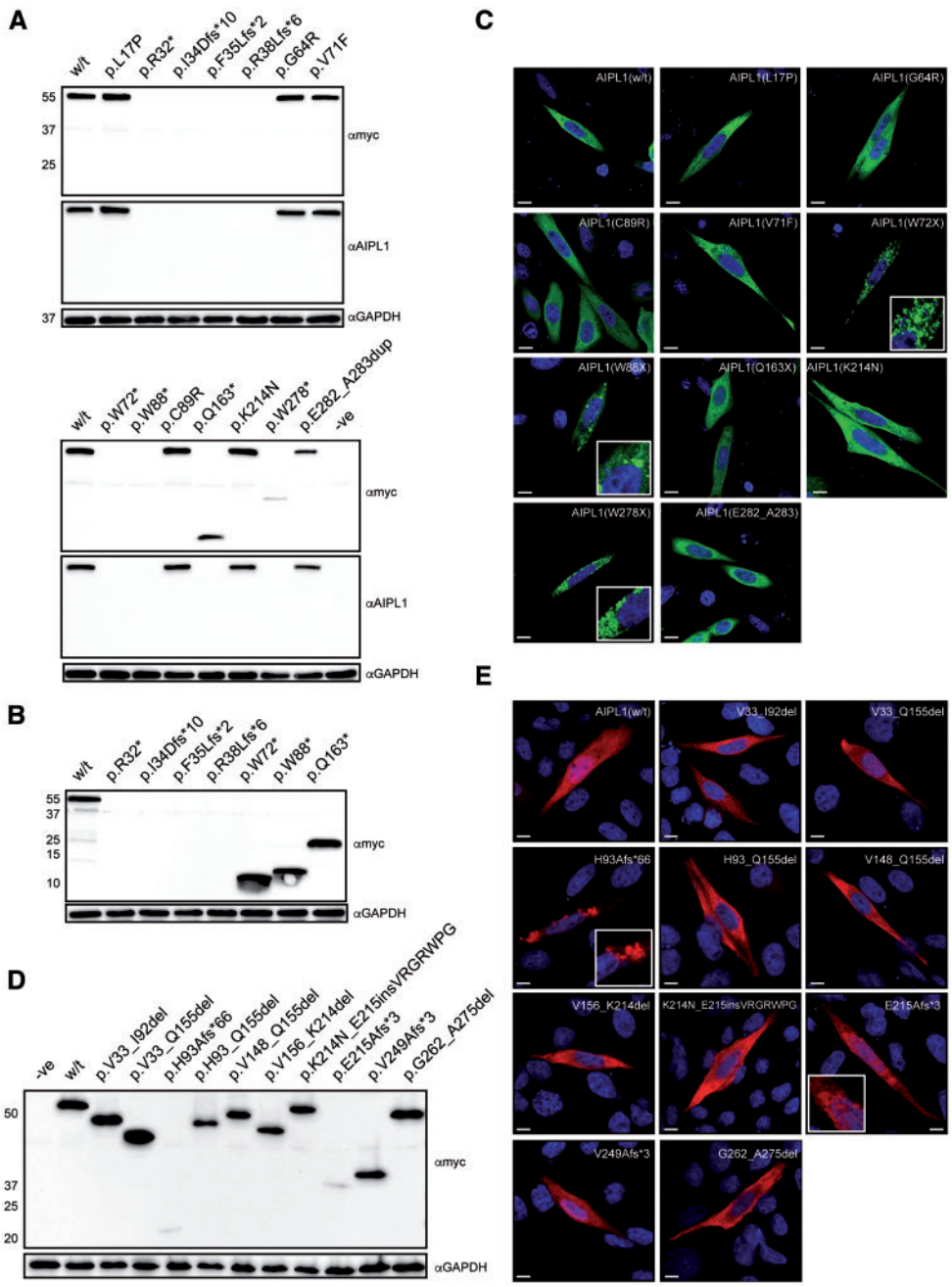

Figure 2. Expression and subcellular localization of AIPL1 variants. (**A**), (**B**) and (**D**) Western blotting analysis of wild-type (w/t) AIPL1 and the indicated AIPL1 variants (A, B) or AIPL1 protein isoforms (D). The proteins were resolved by SDS-PAGE on a 12% (A, D) or 20% (B) gel. The anti-AIPL1 antibody is directed against a C-terminal AIPL1 epitope (7) and the anti-myc antibody recognizes the myc tag fused to the N-terminus of AIPL1. GAPDH was detected as a loading control. (**C**) and (**E**) Indirect immunofluorescent confocal microscopy using anti-myc antibody. The misfolding and aggregation of p.W72*, p.W88*, p.W278*, p.H93Afs*66 and p.E215Afs*3 in visible intracellular inclusions is shown at higher magnification as inserts. Scale bar: 10 μm.

normalized to the expression of the variant in the cell lysate and calculated relative to w/t AIPL1. The ELISA assay corroborated the findings of the Y2H assay, confirming that p.L17P, p.C89R and p.E282_A283dup are significantly impaired in their ability to interact with HSP90α/β compared with w/t AIPL1, while p.V71F, p.K214N and p.G262S are less severely compromised in their ability to bind HSP90α/β. Interestingly, while p.G64R was able to interact with HSP90 in the Y2H assay to induce growth, it is clear from the quantitative ELISA assay that the affinity of binding was reduced compared with w/t AIPL1. Hence, there is a threshold for AIPL1 HSP90 interaction below which growth is not induced in the Y2H assay, with the quantitative ELISA able to discriminate deficiencies in interaction. Interestingly, whilst p.Q163* was able to interact with HSP90 in a TPR-independent manner in the Y2H assay, the interaction of p.Q163* and HSP90α/β was completely abolished in the ELISA assay. Finally, addition of the MEEVD peptide reduced, but did not abolish, the interaction of all the HSP90α/β interacting AIPL1 variants, except for p.C89R where peptide competition was less efficient.

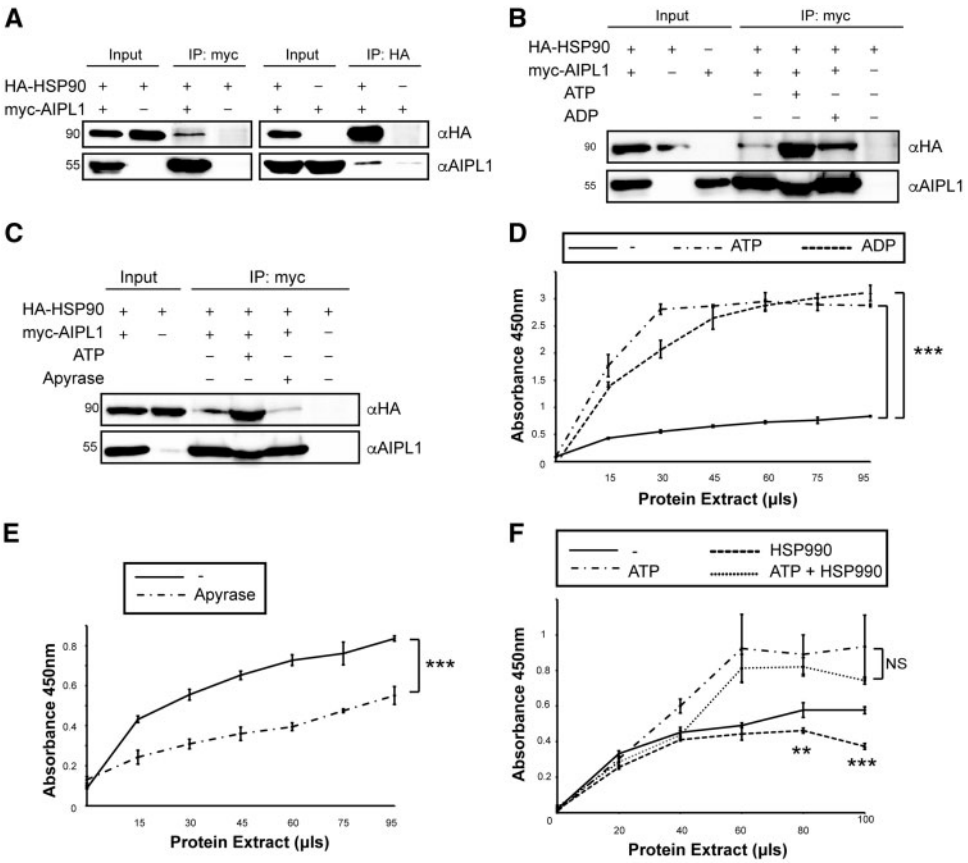

Figure 3. Nucleotide-dependent interaction of AIPL1 with HSP90. (**A**), (**B**) and (**C**) Western blotting analysis of the co-immunoprecipitation of HA-HSP90 with myc-AIPL1. Protein lysates from co-transfected cells were incubated in the absence of nucleotide (A), in the presence of ATP (5 mM) (B), ADP (5 mM) (B) or apyrase (10 units/ml) (**C**). Myc-AIPL1 and HA-HSP90 were immunoprecipitated using anti-myc and anti-HA, respectively. Immunodetection was performed with anti-AIPL1 or anti-HA antibodies. (**D**), (**E**) and (**F**) Quantitative ELISA binding assay of the interaction of myc-AIPL1 with purified human recombinant HSP90α. Increasing volumes of myc-AIPL1 expressing cell lysates were added to a constant concentration of HSP90α (80 nM). When indicated, incubation was done in the presence of ATP (5 mM) (D, F), ADP (5 mM) (D), apyrase (10 units/ml) (E) or HSP990 (5 mM) (F). Statistically significant differences are indicated by 2 ($p \leq 0.01$) or 3 ($p \leq 0.001$) asterisks.

Next, we investigated the interaction of the AIPL1 in-frame domain deletions and frameshift stop mutations expressed from the *AIPL1* splice variations (Fig. 5). None of the AIPL1 variants were able to interact with HSP90 in directed Y2H assays with the exception of p.V33_Q155del (in-frame deletion of exons 2 and 3) and p.K214N_E215insVRGRWPG (Fig. 5A). p.K214N_E215insVRGRWPG mediated a TPR-dependent interaction with HSP90 similar to w/t AIPL1 despite the insertion of seven residues in the loop connecting consecutive TPR motifs in the TPR domain. On the other hand, the recognition of p.V33_Q155del by HSP90 in this assay did not require the MEEVD motif, deletion of which did not compromise the interaction of p.V33_Q155del with HSP90. All the AIPL1 products were expressed in yeast (Fig. 5B), except for p.H93Afs*66. Moreover, both p.H93Afs*66 and p.E215Afs*3 formed intracellular aggregates of misfolded proteins in cells (Fig. 2E) and, accordingly, were unable to rescue growth at the restrictive temperature in directed Y2H assays with HSP90 and HSP90ΔMEEVD (Fig. 5A). The quantitative ELISA (Fig. 5C) confirmed that all of the AIPL1 variants were unable to interact efficiently with HSP90α/β with the exception of p.V33_Q155del which was comparable to w/t AIPL1. The interaction of p.V148_Q155del, p.V156_K214del, p.V249Afs*3 and p.G262_A275del was effectively abolished, while that of p.V33_I92del, p.H93_Q155del and p.K214N_E215insVRGRWPG was significantly reduced compared with w/t AIPL1. However, the efficiency of p.K214N_E215in sVRGRWPG interaction was significantly better than p.V33_I92del and p.H93_Q155del, and p.K214N_E215insVRGRWPG surpassed the threshold for growth in the Y2H assay. MEEVD peptide competition was evident only in the case of w/t AIPL1 and the HSP90α/β interacting products p.V33_Q155del and p.K214N_E215insVRGRWPG, suggesting that features directing the prototypical TPR co-chaperone chaperone interaction are preserved in these variants.

Mutations in the FKBP-like and TPR domain compromise the ability of AIPL1 to stabilize PDE6α in the cytosol

We investigated the impact of the AIPL1 variants on the stabilization of PDE6α in the cytosol and on the activity of the PDE6 holoenzyme to gain further insight into how the independently folded FKBP-like and TPR domains of AIPL1 contribute to rod cGMP PDE6 processing and activity. We first examined the localization of the rod cGMP PDE6 subunits expressed alone and in combination, both in the absence and presence of AIPL1. When expressed alone, PDE6α and PDE6β (Fig. 6A) localized to intracellular membranes, whilst PDE6γ (Fig. 6A) and AIPL1 (Fig. 2) were ubiquitously distributed throughout the cytosol. PDE6α and PDE6β are targeted to and dock at the cytosolic face of the endoplasmic reticulum (ER) following their isoprenylation in the cytosol (40), and their subcellular localization thus overlapped with that of the ER-resident chaperones binding immunoglobulin protein (BiP) and calnexin or the ER retention signal

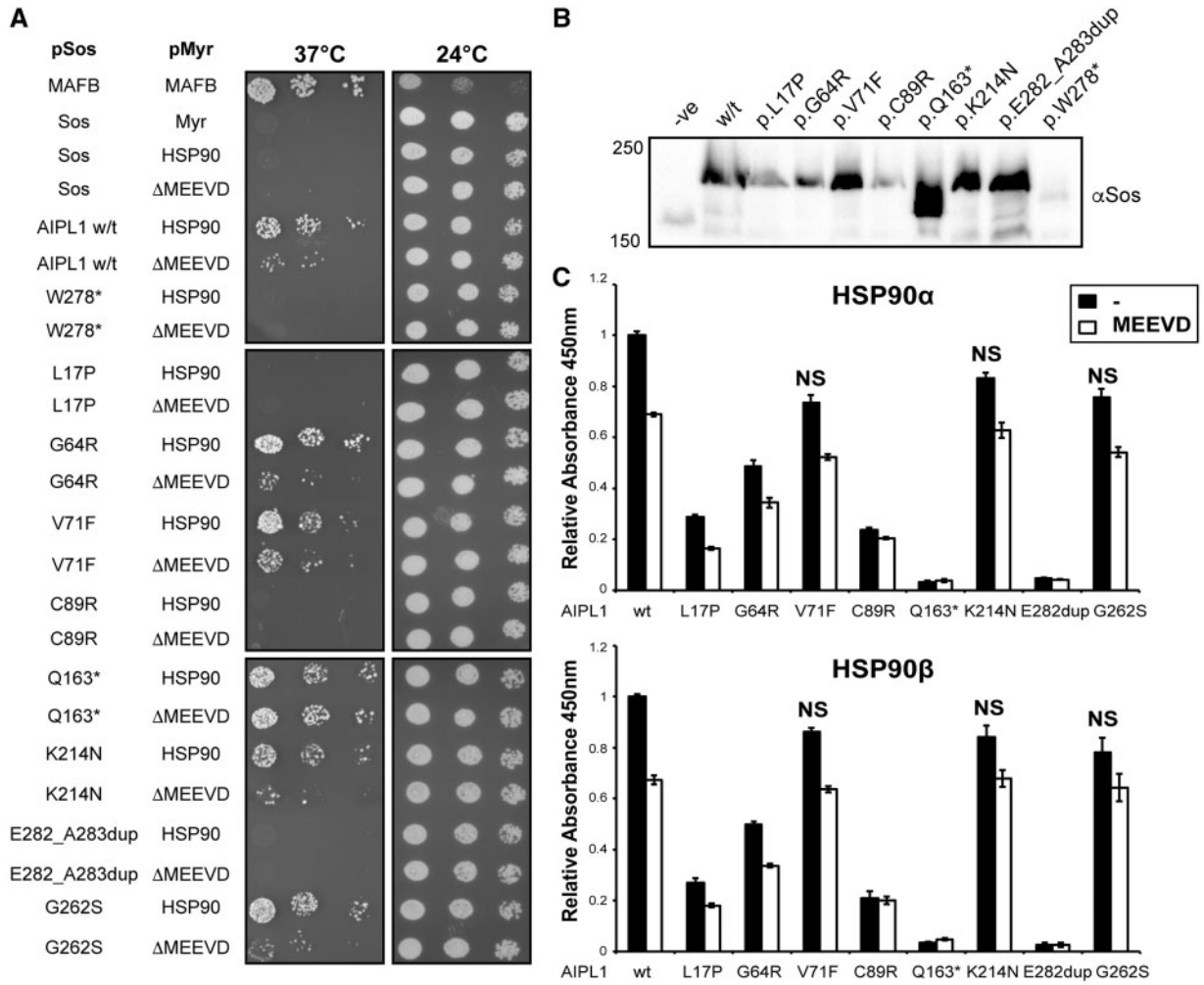

Figure 4. Interaction of LCA-linked AIPL1 variants with HSP90. (**A**) Qualitative analysis of the interaction between AIPL1 and HSP90 through directed Y2H assays. Yeast cdc25H strain was co-transformed with pMyr bearing bovine HSP90α(204–733) or HSP90α(204–733ΔMEEVD) and pSos bearing wild-type (w/t) AIPL1 or the AIPL1 variants indicated. Serial dilutions were tested for their ability to grow on selective media under permissive (24 °C) or restrictive (37 °C) conditions, respectively. (**B**) Western blotting analysis of protein expression in yeast cell extracts of AIPL1 variants using anti-Sos antibody. (**C**) Quantitative ELISA analysis of the interaction between w/t AIPL1 or the AIPL1 variants indicated with purified human recombinant HSP90α and β. The absorbance of each interaction was normalized to the expression level detected by western-blotting and plotted relative to w/t AIPL1 = 1.0. White bars indicate addition of purified MEEVD peptide for competitive binding to AIPL1. Assays were performed in triplicates. All AIPL1 variants showed statistically significant differences ($p \leq 0.01$) with respect to w/t AIPL1 with the exception of the variants demarcated by NS ($p > 0.01$).

sequence KDEL (Fig. 6B). When co-expressed, PDE6α and PDE6β co-localized at the ER, and PDE6γ was recruited to the ER when co-expressed with either PDE6α or PDE6β (Fig. 6C). When co-expressed, there was no change in the respective subcellular localizations of AIPL1 and PDE6γ in the cytosol (not shown). However, while AIPL1 was recruited to the intracellular ER membranes by PDE6β, AIPL1 induced the redistribution of PDE6α from the ER resulting in the co-localization of AIPL1 and PDE6α in the cytosol (Fig. 6C). When PDE6α, β and γ were co-expressed, all three subunits were targeted to the ER irrespective of the presence of AIPL1 (Fig. 6D).

To characterize the redistribution of PDE6α to the cytosol by AIPL1, we assessed the relocalization of PDE6α in relation to the ER marker BiP as we were unable to triple label cells for PDE6α, AIPL1 and an ER marker due to the lack of suitable antibodies (Fig. 7A). The just another co-localization plugin (JACoP) for ImageJ (41) was used to assess the Pearson's intensity correlation and Manders' overlap coefficient for the co-localization of PDE6α and BiP in the cytoplasm of cells in the absence and presence of AIPL1. In the absence of AIPL1, PDE6α co-localized with BiP (Fig. 7A) ($r = 0.87 \pm 0.01$, $M1 = 0.86 \pm 0.06$ where M1 = fraction PDE6α overlapping BiP). In the presence of AIPL1, there was a significant decrease in the intensity correlation ($r = 0.66 \pm 0.03$, $p < 0.001$) and Manders' overlap coefficient ($M1 = 0.24 \pm 0.03$, $p < 0.001$) of PDE6α and BiP as a result of the redistribution of PDE6α to a homogenous localization throughout the cytosol (Fig. 7A). In agreement with these findings, fractionation of cell lysates co-expressing AIPL1 and PDE6α confirmed that AIPL1 increased the levels of PDE6α in the cytosol, and that this occurred in a proteasome-dependent manner (Fig. 7B). Hence, AIPL1 recruits PDE6α to the cytosol, where AIPL1 stabilizes PDE6α against proteasomal degradation.

We next investigated whether the AIPL1 variants could efficiently mediate the redistribution of PDE6α from the intracellular cell membranes to the cytosol compared with w/t AIPL1 (Fig. 7C). The localization of PDE6α was scored based on the morphological distribution in cells. A perinuclear distribution that was particulate in appearance was scored as ER (Fig. 7A, top),

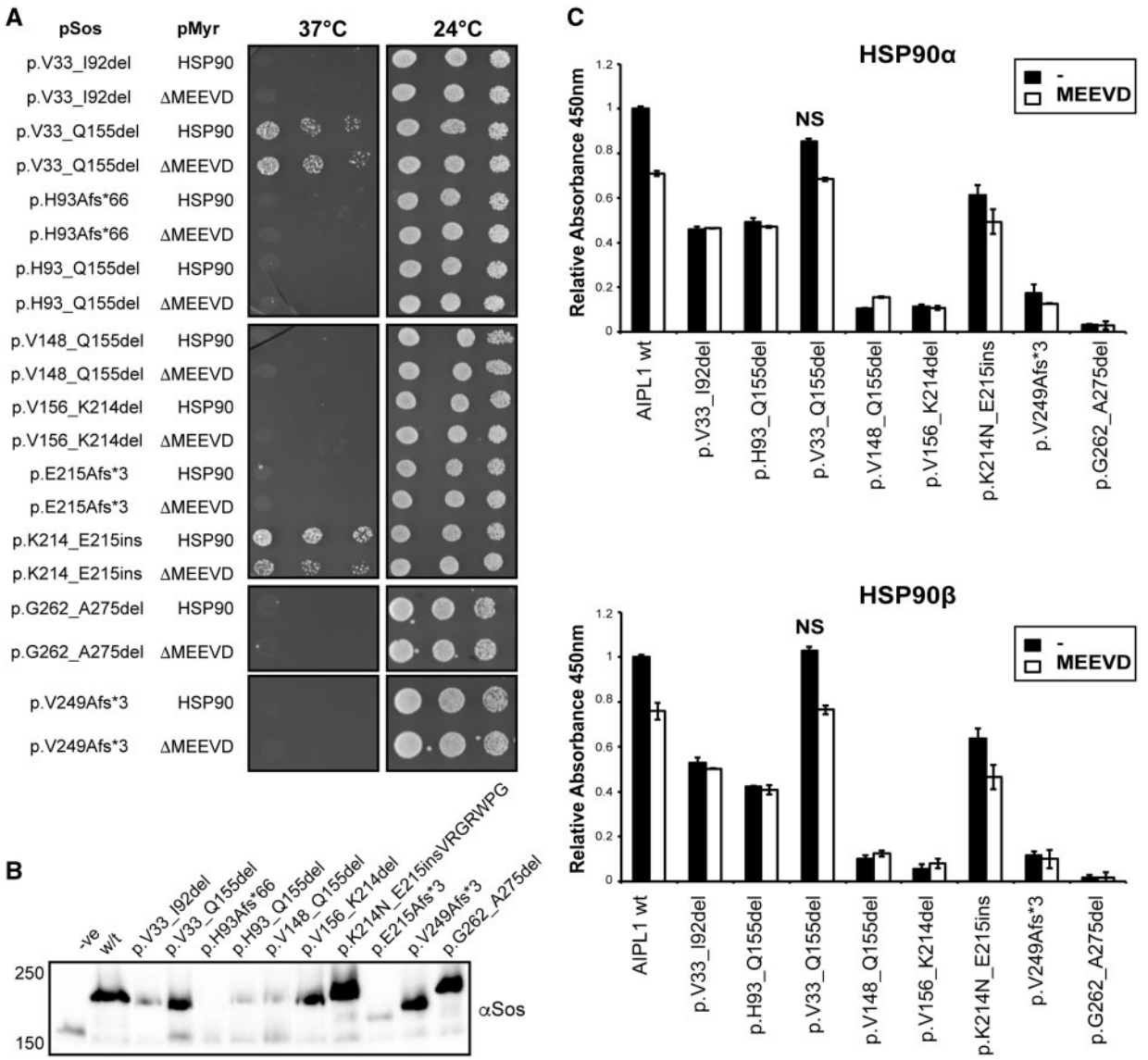

Figure 5. Interaction of LCA-linked AIPL1 protein isoforms with HSP90. (**A**) Qualitative analysis by directed Y2H assays. Yeast cdc25H strain was co-transformed with pMyr-HSP90α(204–733) or pMyr-HSP90α(204–733ΔMEEVD) and pSos bearing wild-type (w/t) AIPL1 or the AIPL1 protein isoforms indicated. Serial dilutions were tested for their ability to grow on selective media at the permissive (24 °C) or restrictive (37 °C) temperature. (**B**) Western blotting analysis of the expression of the AIPL1 protein isoforms in yeast cell extracts using the anti-Sos antibody. (**C**) Quantitative ELISA analysis of the interaction between w/t AIPL1 or the AIPL1 protein isoforms indicated with purified human recombinant HSP90α and β. The absorbance of each interaction was normalized to the expression level detected by western-blotting and plotted relative to w/t AIPL1 = 1.0. White bars indicate addition of purified MEEVD peptide for competitive binding to AIPL1. Assays were performed in triplicates. The differences in binding to HSP90 with respect to w/t AIPL1 were statistically significant ($p \leq 0.01$) for most of the AIPL1 proteins isoforms analysed with the exception of that demarcated by NS ($p > 0.01$).

whereas a smooth homogeneous distribution throughout the cytoplasm was not counted as ER (Fig. 7A, bottom). The percentage of PDE6α expressing cells in which PDE6α localization was scored as ER was quantified and the reciprocal values normalized to w/t AIPL1 to show a deficit in this function (Fig. 7C). Only AIPL1 p.K214N and p.G262S were comparable to w/t AIPL1 in mediating the redistribution of PDE6α to the cytosol, where co-localization with p.K214N and p.G262S was evident (Fig. 7C and D). In contrast, all the remaining AIPL1 variants were unable to efficiently mediate the relocalization of PDE6α to the cytosol compared with w/t AIPL1, and PDE6α remained at the intracellular ER membranes, as exemplified by AIPL1 p.Q163* and p.V33_Q155del (Fig. 7C and D). Importantly, we found that the ability of AIPL1 to redistribute PDE6α to the cytosol and protect PDE6α from proteasomal degradation was dependent on HSP90 as these AIPL1-mediated functions were completely abolished following the inhibition of HSP90 activity with geldanamycin, 17-N-allylamino-17-demethoxygeldanamycin (17-AAG) or HSP990 (Fig. 7E and F).

The regulation of rod cGMP PDE6 activity is compromised by mutations in the AIPL1 FKBP-like and TPR domains

Finally, we investigated the impact of the AIPL1 variants on PDE6 activity (Fig. 8). We conducted our assays in the presence of the holoenzyme as the PDE6γ subunit is critical for the proper

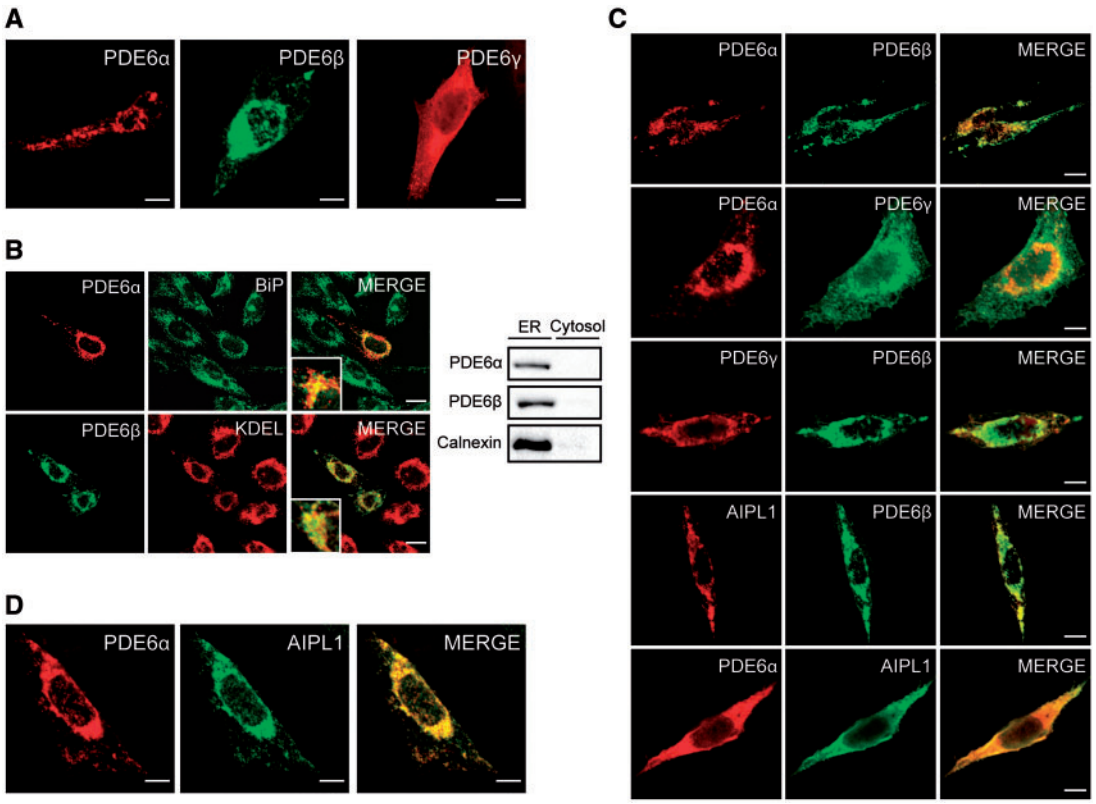

Figure 6. Subcellular localization of rod PDE6 subunits and AIPL1-mediated redistribution of PDE6α. Indirect immunofluorescent confocal microscopy of single (**A** and **B**), double (**C**) or quadruple transfected cells (**D**) with AIPL1, PDE6α, PDE6β and/or PDE6γ subunits as indicated. (A) Localization of PDE6α, PDE6β and PDE6γ in single transfected cells as indicated. (B) Co-localization of PDE6α and PDE6β with the endogenous ER markers BiP and KDEL is shown by immunofluorescence (at higher magnification as inserts), and western blotting shows fractionation with calnexin. (C) Co-localization of AIPL1, PDE6α, PDE6β and PDE6γ as indicated in double transfected cells. PDE6α is targeted to the ER (A and B) but is redistributed to the cytosol in the presence of AIPL1 (C). (D) Co-localization of AIPL1 and PDE6α in quadruple transfected cells. Scale bar: 10 μm.

folding, processing and activity of holoPDE6 *in vivo* (42). In the absence of PDE6, AIPL1 had no effect on the intracellular levels of cGMP in transfected cells, which remained at background level. The PDE6 holoenzyme alone increased cGMP levels above background to a small extent. However, AIPL1 significantly increased the cGMP levels above basal levels. Analysis of the AIPL1 variants from the coding variations (Fig. 8A) revealed that p.L17P and p.G64R were completely unable to modulate PDE6 activity above basal levels, whilst p.V71F, p.C89R and Q163* were severely compromised. In contrast, p.K214N, p.G262S and p.E282_283dup significantly increased PDE6 activity above basal levels, however, p.E282_283dup was not as efficient as w/t AIPL1. Analysis of the AIPL1 variants from the splicing variations (Fig. 8B) revealed that all the variants were significantly and severely impaired in their ability to modulate PDE6 activity compared with w/t AIPL1. Only p.V33_Q155del, p.V156_K214del, p.K214N_E215ins and p.G262_A275del induced a slight increase in cGMP above basal levels. In summary, p.K214N and p.G262S were the most efficient compared with w/t AIPL1 in modulating the basal activity of the PDE6 holoenzyme, whilst the function of all the other AIPL1 variants was compromised to various degrees.

Discussion

AIPL1, a retina-specific HSP90 co-chaperone, facilitates the proper folding and assembly of the visual effector enzyme PDE6. Here, we provide unequivocal experimental evidence that the *AIPL1* variations investigated in this study lead to significant and severe functional deficits in the resultant AIPL1 protein confirming their disease-causing status. In addition, our findings expand the understanding of the role of AIPL1 as a retina-specific chaperone for PDE6 and deliver insights into the molecular mechanisms of pathogenesis associated with these *AIPL1* variations. Such detailed functional studies are lacking in the visual sciences literature and thereby severely limit our understanding of inherited retinal disease, which now presents the commonest cause of blindness in working age adults in UK and the second commonest in childhood.

Our findings are summarized in Figure 9. We first investigated the impact of domain-specific changes in AIPL1 on the interaction with the molecular chaperone HSP90. Structural models of AIPL1 (24,32) confirm that each of the three TPR motifs consists of a pair of anti-parallel α-helices (helix A and B), with sequentially arranged consecutive TPR motifs forming an amphipathic groove proposed to accommodate the terminal EEVD residues of molecular chaperones (Fig. 9). Our data show that disruption of the AIPL1 TPR domain as a result of deletions (p.V156_K214del, p.G262_A275del), insertions (p.K214N_E215 insVRGRWPG), duplications (p.E282_A283dup) or C-terminal truncation (p.V249Afs*3, p.Q163*) compromised the interaction with HSP90 as expected. AIPL1 p.K214N_E215insVRGRWPG was the least compromised of all the AIPL1 TPR domain variants, likely due to the fact that the insertion of seven amino acid

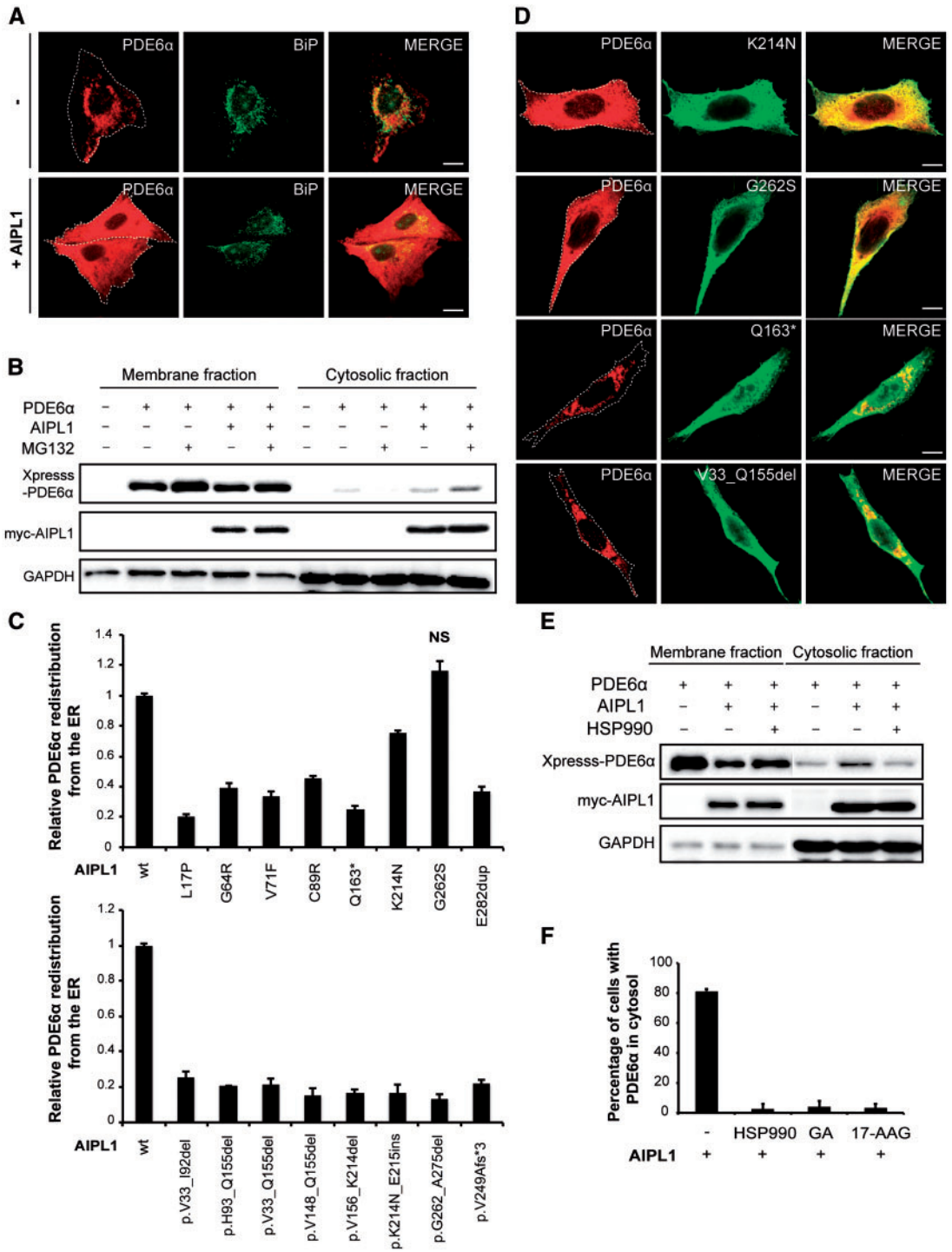

Figure 7. AIPL1-mediated rod PDE6α redistribution from the ER to the cytosol is proteasome dependent and requires HSP90 activity. (A) Immunofluorescent confocal microscopy of PDE6α and endogenous BiP in the absence and presence of AIPL1. The co-localization of PDE6α with BiP was determined using the ImageJ JACoP (41). The cell outlines are demarcated by a white dashed line. (B) Western blotting analysis of PDE6α alone or in the presence of AIPL1 in the membrane and cytosolic fractions, in the absence and presence of proteasome inhibitor (50 μM MG132, 4 h). The anti-Xpress (PDE6α), anti-myc (AIPL1) and anti-GAPDH (loading control) antibodies were used. AIPL1 induces the subcellular relocalization of PDE6α from the ER to the cytosol where it stabilizes PDE6α to proteasomal degradation. (C) Quantitative analysis of the ability of the AIPL1 variants and protein isoforms to redistribute PDE6α to the cytosol compared with w/t AIPL1 = 1. (D) Indirect immunofluorescent confocal microscopy of PDE6α relocalization to the cytosol in the presence of the AIPL1 variants p.K214N, p.G262S, p.Q163* or p.V33_Q155del. (E) Western blotting analysis of PDE6α alone or in the presence of AIPL1 in the membrane and cytosolic fractions, in the absence and presence of the inhibitor HSP990 (1 μM). (F) Quantitative analysis of the ability of AIPL1 to redistribute PDE6α to the cytosol in the absence or presence of the inhibitors HSP990, geldanamycin and 17-AAG (1 μM).

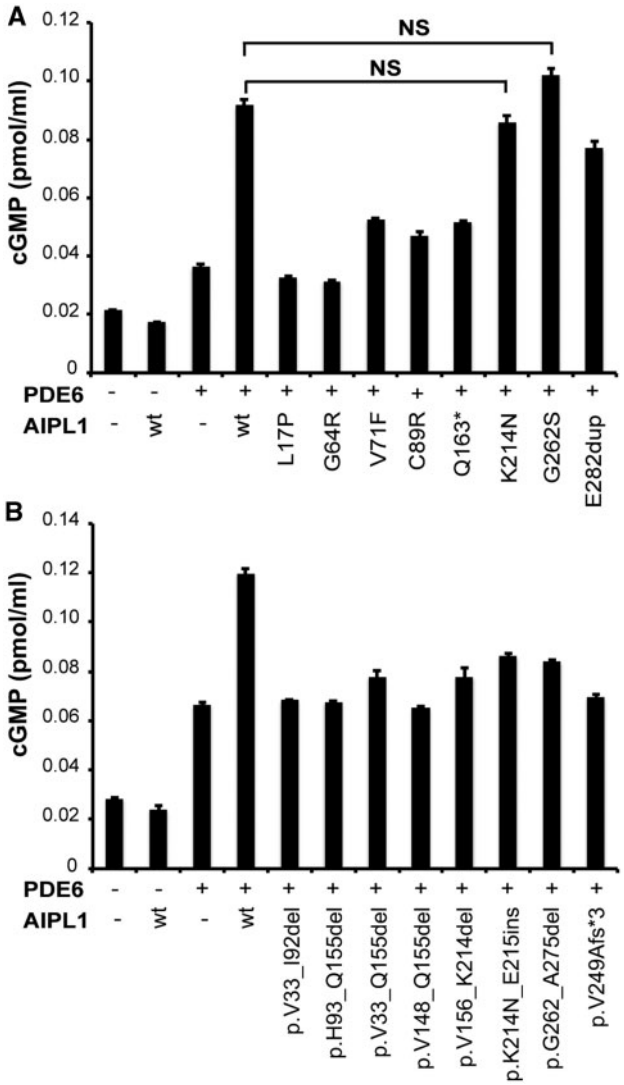

Figure 8. Heterologous rod PDE6 activity in the presence of the AIPL1 variants and protein isoforms. (**A**) and (**B**) Quantitative analysis of the cGMP concentration from cells expressing the PDE6 holoenzyme (α, β and γ) alone, and in the presence of wild-type (w/t) AIPL1, the AIPL1 variants (A) or AIPL1 isoforms (B) as indicated. Assays were performed at least three times and in triplicate. All AIPL1 variants or AIPL1 protein isoforms showed statistically significant differences ($p \leq 0.01$) compared with w/t AIPL1 except p.K214N and p.G262S that did not have a significant effect on PDE6 activity (NS) ($p > 0.05$).

resides in the loop connecting the first and second TPR motifs may have less of an impact on the topological arrangement of these motifs (Fig. 9). On the other hand, the small deletion p.G262_A275del and duplication p.E282_A283dup both completely abolished HSP90 interaction, likely due to their significant impact on the topological packing of the TPR domain. AIPL1 p.G262_A275del leads to the loss of the last two residues of the second TPR motif and almost the entire helix A of the third TPR motif (Fig. 9). Helix A of this TPR motif includes TPR consensus residues required for the antiparallel packing of the helix A and B α-helices, as well as residues predicted to mediate tight electrostatic interactions with the EEVD motif of molecular chaperones through the formation of a peptide-binding pocket (10). Similarly, the duplication of two residues at the beginning of helix B of the third TPR motif in p.E283_A283dup is expected to disrupt the packing of adjacent anti-parallel α-helices of this motif and consequently impair HSP90 interaction. In-frame deletion of the interdomain connecting loop between the FKBP-like and TPR domain and the first TPR motif in p.V156_K214del similarly completely compromised the interaction of AIPL1 with HSP90, as did C-terminal truncation of AIPL1 (p.V249Afs*3 and p.Q163*) (Fig. 9). AIPL1 p.V249Afs*3 is characterized by the loss of the PRD and half of the TPR domain, whilst AIPL1 p.Q163* leads to the loss of the entire TPR domain and PRD (Fig. 9). The rescue of growth by p.Q163* in the Y2H assay irrespective of the deletion of the HSP90 MEEVD motif suggests transactivation by this variant in the Y2H assay. Importantly, our data show that p.V156_K214del and p.K214N_E215insVRGRWPG, the AIPL1 protein isoforms translated as a result of alternative transcription of c.642G > C(p.K214N), have a reduced affinity of binding with HSP90 while the missense variant p.K214N had a minimal effect on the interaction with HSP90 in comparison to wild-type AIPL1. Similarly, p.V249Afs*3, which is produced as a result of alternative transcription from c.784G > A(p.G262S), is also unable to bind HSP90, whereas p.G262S was comparable to wild-type AIPL1 in binding HSP90. This confirms alternative splicing and resultant AIPL1 loss of function as the underlying cause of pathogenesis for AIPL1 p.K214N and p.G262S, and stresses the importance of defective splicing as a disease-causing mechanism.

Our data show that with the exception of p.K214N and p.G262S, all of the AIPL1 TPR domain variants also affect the rod cGMP PDE6 activity (Fig. 9). Similarly, it has been reported that the p.C239R missense variant in the AIPL1 TPR domain leads to the loss of cone PDE6 activity (30). Interestingly, loss of the entire TPR domain in p.Q163* severely compromised the ability of AIPL1 to modulate PDE6α redistribution and the activity of the PDE6 holoenzyme. NMR data reveal that the FKBP-like domain of human AIPL1 can attain the native fold in the absence of the TPR domain and successfully bind a farnesyl moiety (33). In another study, the AIPL1 FKBP-like domain bound a farnesyl probe comparably to full-length AIPL1 in the absence of the TPR domain, which itself was unable to bind the farnesyl probe and did not alter the affinity of the FKBP-like domain for the probe (32). Not only does this suggest that each domain of AIPL1 plays a unique role in chaperoning PDE6 but together with our data also suggest that binding of the farnesyl moiety to the FKBP-like domain alone is not sufficient for AIPL1 to fulfil its role in modulating PDE6 stability and activity, which also requires a functional interaction with HSP90. This is supported by the finding that reciprocal chimeras of the FKBP-like and TPR domains from AIPL1 and AIP, which is unable to bind a farnesyl moiety, both completely failed to modulate the activity of the cone PDE6 holoenzyme (30). It is also interesting that while the small TPR insertion p.K214N_E215insVRGRWPG had a relatively less severe impact on HSP90 interaction, the impact on PDE6 was significant (Fig. 9). Hence, the integrity of this domain and its ability to mediate an interaction with HSP90 is critically important for AIPL1 to fulfil its role in PDE6 stability and activity. In addition to the integrity of each domain, we propose that their relative orientation and organization is also important for the overall function of AIPL1. Structural models of mouse and human AIPL1 revealed that the FKBP-like domain and TPR domain of AIPL1 fold independently with no obvious interdomain contacts and can adopt a range of relative orientations, some of which may be constrained by the length of the flexible interdomain loop connecting the FKBP-like and TPR domain (24,32). The proposed importance of the integrity and orientation of both domains is supported by our findings that missense changes and in-frame deletions in the AIPL1 FKBP-like domain

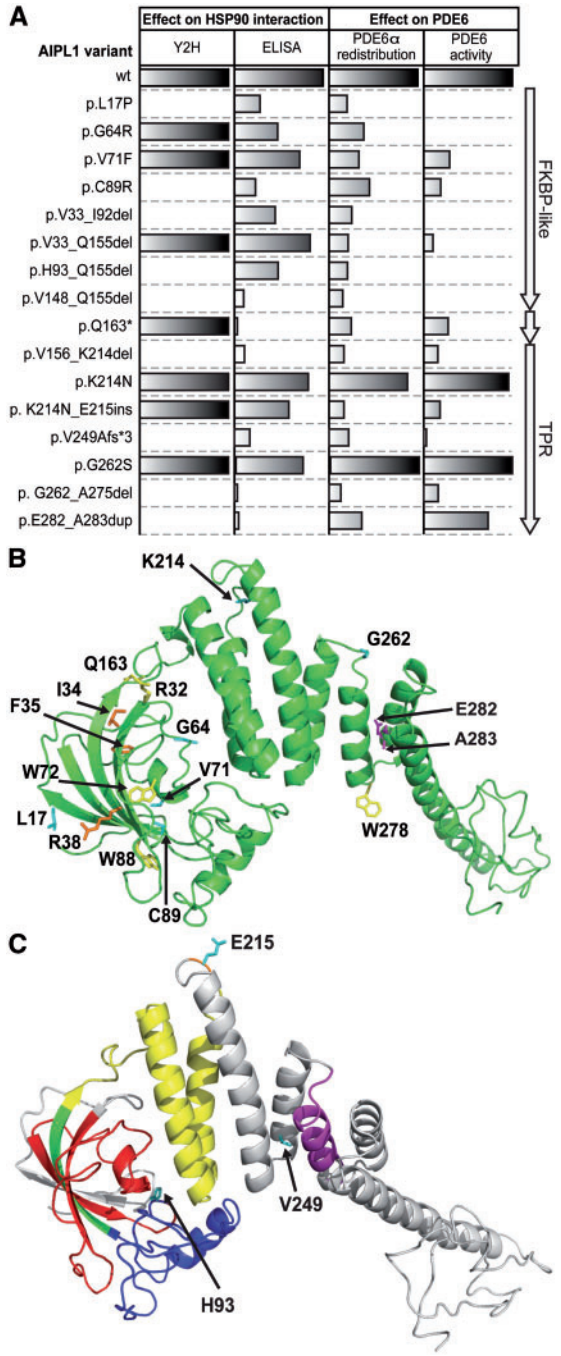

Figure 9. Summary of the functional impacts of the AIPL1 variants. (**A**) Summary of the effect of the AIPL1 variants on HSP90 interaction, PDE6α redistribution and PDE6 activity. (**B**) Pymol cartoon showing position of AIPL1 mutations: AIPL1 (green) with the position of missense (p.L17P, p.G64R, p.V71F, p.C89R, p.K214N, p.G262S, cyan sticks), nonsense (p.R32*, p.W72*, p.W88*, p.Q163*, p.W278*, yellow sticks) and frameshift premature translation mutations (p.F35Lfs*2, p.I34Dfs*10 and p.R38Lfs*6, orange sticks) is shown. Magenta sticks show the position of the duplication (p.E282_A283dup). (**C**) AIPL1 (grey) with regions of structure coloured to indicate deletions, insertions and frameshift premature translation mutations resulting from aberrant *AIPL1* splicing. p.V33_I92del (in-frame deletion of exon 2), red; p.H93_Q155del (in-frame deletion of exon 3), blue + green; p.V33_Q155 (in-frame deletion of exons 2 and 3), red + blue + green; p.V148_Q155, green; p.V156_K214del, yellow; p.K214N_E215insVRGRWPG, orange; p.G262_A275del, magenta. H93Afs*66, E215Afs*3 and V249Afs*3 represent points of frameshift leading to the inclusion of non-AIPL1 sequences and early termination, cyan sticks. The model of AIPL1 (B and C) was built using Phyre2 (48).

conversely compromise the ability of AIPL1 to interact with HSP90 (Fig. 9).

Structural data reveal that the typical FKBP fold is conserved in human AIPL1 and is composed of an α-helix surrounded by a five-stranded β-sheet to create a hydrophobic cavity analogous to the FKBP ligand-binding site (24,33) (Fig. 9). The FKBP-like domain of AIP and AIPL1 uniquely contain an intervening loop between the fourth and fifth strands of the β-sheet thought to occlude the hydrophobic cavity of the FKBP-like domain and influence the relative domain orientation by engaging in steric clashes with the TPR domain (24,33,44). The FKBP-like domain missense variants p.L17P, p.G64R and p.C89R were unable to efficiently modulate PDE6 activity and were also inefficient at binding HSP90 (Fig. 9). The missense variant p.V71F was also unable to modulate PDE6 activity but was the least compromised in binding HSP90 compared with the other missense variants. AIPL1 p.V71F has been reported to bind a farnesyl moiety comparably to wild-type AIPL1 and circular dichroism (CD) spectra revealed that there are no global conformational changes in the mutant protein (32). Yet, p.V71F was deficient in driving cGMP hydrolysis by cone PDE6 (30), suggesting that farnesyl binding alone is not sufficient for the overall function of AIPL1. Like p.V71F, CD analysis of p.C89R ruled out global conformational changes of the mutant protein (32), however, both these residues are embedded in the core FKBP domain and may alter or destabilize the FKBP fold (Fig. 9). AIPL1 p.C89R has been reported to drastically reduce the interaction of AIPL1 with a farnesyl motif and consequently severely impair the activity of cone PDE6 (30,32). Similarly, we found that p.C89R was severely impaired in the ability not only to modulate rod PDE6 activity but also to bind HSP90. The residues C89 and L147 are in close proximity in a hydrophobic pocket in the structural model of AIPL1 and flank the beginning and end, respectively, of the unique insert region of the FKBP-like domain (32,33). It was proposed that C89 and L147 are essential for the conformation of the insert region that may play a direct and critical role in farnesyl binding. Interestingly, a direct but weak and transient interaction was reported to be mediated by residues in the analogous unique insert region of AIP and HSP90, thereby rendering the FKBP-like ligand binding domain accessible (44). Hence, missense mutations in the AIPL1 FKBP-like domain may compromise the integrity of the FKBP fold and the interaction with the isoprenyl motif, alter the requisite domain orientations and reduce the efficiency of HSP90 interaction. Similarly, p.L17P and p.G64R are highly conserved residues that are likely to be of structural or functional importance (Fig. 9).

Notably, in-frame deletions in the AIPL1 FKBP-like domain similarly significantly impaired the interaction with HSP90. The in-frame deletions p.V33_I92del (in-frame deletion of exon 2) and p.H93_Q155del (in-frame deletion of exon 3) result in the loss, respectively, of the first and second halves of the unique insert region and are therefore likely to have a significant impact on the integrity of the FKBP fold, farnesyl binding or the relative orientation of the FKBP-like domain (Fig. 9). Deletion of only eight residues (p.V148_Q155del) near the interdomain connecting linker between the FKBP-like and TPR domain severely compromised AIPL1 activity in relation to both PDE6 and HSP90, suggesting this may have a very significant and severe effect on the relative orientations of the two domains. AIPL1 p.H93_Q155del and p.V148_Q155del are the resultant protein isoforms from alternative transcription of c.465G > T(p.Q155H), confirming aberrant transcription with a consequent impact on protein function as the underlying cause of pathogenesis for this *AIPL1* variation. Finally, a large 122-residue in-frame deletion of the entire FKBP-like domain in p.V33_Q155del (in-frame deletion of exons 2 and 3) was completely deficient in modulating PDE6 activity but retained

the ability to interact with HSP90 (Fig. 9). This suggests that the TPR domain of AIPL1 in isolation can mediate an interaction with HSP90, as conversely the FKBP-like domain in isolation can mediate an interaction with farnesyl, but efficient binding of both are required for PDE6 activity.

In agreement with previously published data (24), we detected an increase in cGMP concentrations in the presence of AIPL1 following heterologous reconstitution of the rod PDE6 holoenzyme. Similarly, it was previously reported that AIPL1 could interact with the assembled rod PDE6 holoenzyme to inhibit the basal activity, and that AIPL1 had no effect on the catalytic activity following limited proteolysis of the rod PDE6γ subunits (24). In contrast, AIPL1 enhanced the catalytic activity of the heterologously reconstituted cone PDE6 holoenzyme, and this occurred more efficiently following trypsin treatment to relieve the PDE6γ inhibition of the catalytic cone PDE6α' subunits (30). Although cone PDE6 is found predominantly in soluble retinal fractions, rod PDE6 is predominantly found at the membrane mediated primarily by the geranylgeranylated C-terminus of rod PDE6β (45). Hence, the mechanism of AIPL1 action during rod and cone PDE6 assembly and activity may differ to accommodate these differences between rod and cone PDE6. We confirm here that the interaction of AIPL1 and HSP90 is critically important to facilitate the stable assembly of the rod PDE6 holoenzyme. Our data confirm that AIPL1 promotes the stability of PDE6α in the cytosol in an HSP90-dependent manner and protects PDE6α from proteasomal degradation, as seen in *ex vivo* retinal explants from the *Aipl1* knockout mice (27). AIPL1 can bind to the assembled rod PDE6 holoenzyme (24) and may inhibit the catalytic activity until targeted translocation to the outer segment is achieved via delivery to the connecting cilium. This mechanism is analogous to that involving the role of HSP90 and substrate-specific TPR domain co-chaperones in the functional maturation and targeted translocation of other HSP90 substrates. However, while AIPL1 and HSP90 play a very important role in the stable assembly of the PDE6 holoenzyme, the mode of delivery to the connecting cilium is still unknown.

In summary, we conclude that the integrity of the FKBP-like domain and the TPR domain of AIPL1, as well as their relative orientation or organization is critical for AIPL1 to fulfil its function as a retinal chaperone for PDE6 in conjunction with HSP90. Moreover, the function of AIPL1 in rod PDE6 assembly and activity is fundamentally dependent on HSP90. Future cellular and structural studies will be necessary to fully understand the requisite domain orientations and regulation thereof.

Materials and Methods

AIPL1 nomenclature

The *AIPL1* exon numbering is according to the Ensembl Transcript ENST00000381129 (RefSeq NM_014336, NP_055151). Nomenclature of *AIPL1* sequence variants followed Human Genome Variation Society guidelines.

Cell culture and transfection

Chinese hampster ovary and human embryonic kidney (HEK293T) cells were grown in Dulbecco's modified Eagle's medium (DMEM)/F12 or DMEM, respectively, (Invitrogen) with 10% heat inactivated fetal bovine serum, 100 units/ml of penicillin and 100 μg/ml of streptomycin with an atmosphere of 6% CO_2 at 37°C. For maintenance, cells were passaged every 3–4 days. Cells were seeded into eight-well chamber slides (3.5×10^4 cells per well) or into six-well plates (5×10^5 cells per well) for immunofluorescence and western blotting, respectively. Cells were transfected using TransIT-LT1 transfection reagent according to the manufacturer's instructions (Mirus). Where indicated, the HSP90 inhibitor HSP990 (1 μM) (Novartis) or the proteasome inhibitor MG132 (50 μM) (Enzo Life Sciences) were added to the cell cultures.

Microorganisms

For cloning and amplification of plasmid DNA, the *Escherichia coli* strain DH5α [*fhuA2* Δ(*argF-lacZ*)*U169 phoA glnV44* Φ*80* Δ(*lacZ*)*M15 gyrA96 recA1 relA1 endA1 thi-1 hsdR17*] from New England Biolabs (NEB) was used. The *Saccharomyces cerevisiae* strain cdc25H (Matα ura3-52 his3-200 ade2-101 lys2-801 trp1-901 leu2-3 112 cdc25-2 Gal^+) from CytoTrapXR (Stratagene) was used to perform Y2H assays.

DNA manipulation and plasmids

General DNA methods were performed using standard techniques. To express myc-tagged AIPL1 in cells, pCMV-Tag3C-*AIPL1* was used (38). Plasmid pcDNA3-HA-*HSP90β* was a gift from William Sessa (Addgene plasmid # 22 487). For the Y2H assays the plasmid pSos-*AIPL1*, pMyr-*HSP90α*(204–733) and pMyr-*HSP90α*ΔMEEVD(204–728) were used (10). Mutagenesis of specific residues in *AIPL1* were carried out by PCR site-directed mutagenesis using the Q5 Site-Directed Mutagenesis Kit (NEB). All plasmids were confirmed by Sanger sequencing (Source Bioscience).

Cloning of rod PDE6 expression constructs

The cDNAs of rod PDE6α and PDE6γ subunits were amplified by PCR using human retina cDNA (Clontech) as template, PDE6β cDNA was amplified from WERI-Rb-1 cDNA. Primers used for PCR were AA-325 (5′-CGGGGTACCTGGCGAGGTGACAGCAGAG GAGG-3′) and AA-326 (5′-CATCCAAGTCCTGCTGCATCCAGTAA TCTAGACTAG-3′) for amplification of PDE6α, AA-331 (5′ CGA ATTCGGTCGACCAGCCTCAGTGAGGAGCAGGCCCGGAGC-3′) and AA-332 (5′-GCACCCAAGTCTTCAACCTGCTGTATCCTGTGACTCG AGCGG-3′) for amplification of PDE6β, and AA-329 (5′-CCG GAATTCGGAACCTGGAACCGCCCAAGGCTGAG-3′) and AA-330 (5′-GCTGGCCCAATATGGCATCATCTAGGGTACCCCG -3′) for amplification of PDE6γ. PDE6α was inserted into pcDNA3.1-His/-A (Invitrogen) using restriction sites KpnI/XbaI, PDE6β was inserted into pCMV-HA (Clontech) using restriction sites SalI/XhoI, and PDE6γ was inserted into pCMV-myc (Clontech) using restriction sites EcoRI/KpnI. All constructs were verified by sequencing (Microsynth AG, Balgach, Switzerland).

Y2H assays

Assays were performed according to the manufacturer's instructions (CytoTrapXR; Stratagene). The vectors pMyr and pSos or their derivatives were co-transformed using the lithium acetate method (46) into the temperature-sensitive mutant strain cdc25Hα. Yeast co-transformants were selected on synthetic dextrose (SD) medium deficient for uracil and leucine (-UL). To perform qualitative analysis of the two-hybrid interactions, at least three colonies from every co-transformation were cultured overnight in selective liquid SD medium (-UL) and growing cultures were adjusted to an optical density at 600 nm (A_{600}) of 0.5.

Serial 1:10 dilutions of the yeast cultures were prepared and the cellular suspensions were spotted onto synthetic galactose plates lacking -UL. Growth was monitored at 24°C and at the restrictive temperature of 37°C. Various pSos and pMyr constructs provided with the two-hybrid system were used as controls for positive and negative interactions. Protein expression was verified according to the manufacturer's instructions by resolving yeast cell extracts obtained through the trichloroacetic acid precipitation method by SDS-PAGE, followed by western blotting using the anti-Sos antibody (1:250) (Transduction Laboratories).

Immunocytochemistry

Twenty-four hours after transfection, cells were fixed with 4% paraformaldehyde for 10 min and permeabilized in 0.5% Triton X-100 for 10 min. Non-specific binding was blocked using 3% bovine serum albumin (BSA), 10% donkey serum in PBS for 1 h at room temperature. Cells were then incubated for 1 h with either mouse monoclonal anti-myc (1:500) (clone 9E10, Sigma), monoclonal mouse anti-Xpress (1:100) (Invitrogen), rabbit monoclonal anti-PDE6β (1:500) (ThermoFisher Scientific) or rabbit polyclonal antisera anti-AIPL1 (1:250) (38), mouse monoclonal anti-KDEL (1:250) (clone 10C3, Enzo Life Sciences) or rabbit anti-GRP78/BiP (1:250) (GL-19, Sigma). Primary antibody incubation was followed by three washes with PBS and a 1 h incubation with secondary antibodies, Cy3-conjugated donkey anti-mouse (1:100) (Jackson ImmnoResearch), donkey anti-mouse Alexa 594 (1:600) (ThermoFisher Scientific) or donkey anti-rabbit Alexa 488 (1:600) (ThermoFisher Scientific). Cells were washed three times in PBS and incubated with 4',6-diamidino-2-phenylindole (DAPI) (2 mg/ml) for 5 min, mounted in fluorescent mounting medium (Dako) and visualized with a Zeiss LSM710 laser scanning confocal microscope. The images were exported from LSM Browser and prepared using ImageJ and Adobe Photoshop.

Cells extracts and immunoblotting

Transfected cells were washed twice in cold PBS and incubated for 10 min in radioimmunoprecipitation assay buffer (50 mM Tris–HCl pH 7.5, 150 mM NaCl, 1 mM EDTA, 1% NP-40, 0.5% sodium deoxycholate, 0.1% SDS) with 2% protease inhibitor cocktail (Sigma) at 4°C. Cell lysates were sonicated and centrifuged at 13 000rpm for 30 min at 4°C. The protein concentration in the soluble fraction was determined using the bicinchoninic acid assay (ThermoScientific) and then normalized to the same amount using 2× Laemmli sample buffer. For subcellular fractionation, cell lysis was performed in isotonic buffer (10 mM Tris–HCl pH 7.4, 2 mM EDTA, 250 mM sucrose) using a syringe and a 20 gauge needle followed by centrifugation at 90 000*g* to obtain a cytosolic and ER-enriched fraction. Protein extracts were resolved by denaturing SDS-PAGE and transferred onto nitrocellulose membranes. Immunodetection of myc-tagged proteins was carried out using mouse monoclonal anti-myc (1:1000) (clone 9E10, Sigma). Rabbit polyclonal (Y-11) anti-HA antibody (1:1000) was purchased from Santa Cruz Biotechnology. Rabbit polyclonal antisera anti-AIPL1 (1:1000) (Ab-hAIPL1) has been described previously (38). PDE6α and PDE6β were detected with mouse monoclonal anti-Xpress (1:250) and rabbit polyclonal anti-PDE6β (1:1000), respectively, from Thermo Scientific. The expression of ER markers was detected using rabbit polyclonal anti-calnexin (1:1000) from Enzo Life Sciences. Loading controls were detected using mouse monoclonal anti-glyceraldehyde 3-phosphate dehydrogenase (1:30 000) from Sigma. Goat anti-mouse (1:30 000) and anti-rabbit (1:30 000) secondary antibodies conjugated with horseradish peroxidase were from Pierce Biotechnology. The ECL plus enhanced (GE Healthcare) or the Luminata Crescendo (Millipore) chemiluminescent detection reagents were used according to the manufacturer's instructions. Western blot densitometry was performed using ImageJ.

Immunoprecipitation

Twenty-four hours after transfection, cells were lysed in 20 mM Tris–HCl pH 7.5, 100 mM NaCl, 5 mM $MgCl_2$, 0.5% Triton X-100, 1 mM phenylmethylsulfonyl fluoride, 2% protease inhibitor cocktail. Myc-AIPL1 and HA-HSP90 were immunoprecipitated using mouse monoclonal anti-myc (1:250) (clone 9E10, Sigma) or mouse monoclonal anti-HA (1:250) (HA-7, Sigma) for 1–2 h at 4°C with rotation. The immunoprecipitates were incubated with 30 µl of Dynabeads Protein G (Invitrogen) for 1 h. Beads were washed extensively with the same buffer, resuspended in 2× Laemmli sample buffer, and proteins analysed by SDS-PAGE and immunoblotting as described earlier. Where indicated, 5 mM ATP (Sigma), 5 mM ADP (Sigma) or Apyrase (10 units/ml) (NEB) were added to the lysates just before incubating with the antibodies.

HSP90 ELISA

The assays were performed in Immulon 4HBX 96-well plates (Fisher Scientific). Expression and purification of the His-tagged human HSP90α and β, was performed as previously described (47). HSP90α (80 nM) or HSP90β (80 nM) in 100 mM $NaHCO_3$ pH 8.5 was added to the wells (100 µl/well) and incubated at 4°C for 1 h. BSA was added to adjacent wells at a concentration of 0.1% (w/v) as a control for non-specific binding. Wells were blocked with 1% blocking reagent (Sigma) in 100 mM $NaHCO_3$ pH 8.5 (300 µl/well) for 1 h at 4°C and then washed three times with chilled TBST (50 mM Tris–HCl pH 7.5, 150 mM NaCl, 0.075% Tween-20) to remove excess of protein. Cell lysates from transfected cells were added to the wells in lysis buffer (20 mM Tris–HCl pH 7.5, 100 mM NaCl, 5 mM $MgCl_2$, 0.075% Tween-20) containing 2% of protease inhibitor cocktail. Increasing volumes of myc-AIPL1 expressing cell lysate (from 10 to 100 µl) was added to lysis buffer to a final volume of 100 µl to determine the kinetics of the interaction of myc-AIPL1 with HSP90α/β. For comparison of the AIPL1 variants to w/t AIPL1, 50 µl cell lysates were added to lysis buffer to a final volume of 100 µl. After 1 h of incubation at 4°C, the wells were washed five times with chilled lysis buffer (200 µl/well). Mouse anti-myc antibody (clone 9E10, Sigma) (1:1000) in lysis buffer containing 0.1% blocking reagent was then added to each well for 1 h (100 µl/well). After five washes, the anti-mouse HRP conjugated antibody (1:10 000) was added and incubated for another hour. After five final washes, the substrate 3,3′,5,5′-tetramethylbenzidine (Sigma) (100 µl/well) was added for colorimetric detection and the plate incubated at 30°C for 30 min with shaking. The reaction was stopped with an equal volume of 0.5 M H_2SO_4 and the absorbance measured at 450 nm. For comparison of the AIPL1 variants to w/t AIPL1, the absorbance measured at 450 nm was normalized to the expression level in cell lysates detected by SDS-PAGE and western blotting. Where indicated, 5 mM ATP (Sigma), 5 mM ADP (Sigma), Apyrase (10 units/ml) (NEB) or HSP990 inhibitor (5 mM) (Novartis) were used. All assays were done in triplicates and repeated at least three times. Competition assays were performed adding the purified MEEVD pentapeptide from Biomatik at a final concentration of 100 µM to the cell lysates in the 96-well plate.

Quantification of PDE6α localization

To quantify the relocalization of PDE6α by AIPL1, pcDNA3.1AXpress-*PDE6α* was transfected in 8-well chamber slides in the absence or presence of pCMV-Tag3C-*AIPL1* and immunocytochemistry performed as described to detect the endogenous ER marker BiP (rabbit anti-GRP78/BiP) and PDE6α (anti-Xpress antibody). The JACoP for ImageJ (41) was used as described (43) to measure the co-localization of PDE6α with BiP in the cytoplasm in the absence and presence of AIPL1. To quantify the effect of the AIPL1 variants on PDE6α localization, pCMV-Tag3C-*AIPL1* and pcDNA3.1AXpress-*PDE6α* were co-transfected in 8-well chamber slides and immunocytochemistry performed as described to detect AIPL1 (anti-AIPL1 antibody) and PDE6α (anti-Xpress antibody). The total number of cells in which PDE6α localized to the ER was counted as a percentage of the total number of cells expressing PDE6α. Three groups of ∼50 PDE6α expressing cells were counted by moving consecutively from one non-overlapping field to the adjacent contiguous field. The counting was conducted blind to the identity of the AIPL1 variant co-transfected and the experiment was repeated at least three times. To illustrate a deficit in the ability of AIPL1 to redistribute PDE6α from the ER to the cytosol, the data was transformed as follows: the reciprocal of the percentage was calculated and multiplied by 100, after which all data was normalized to w/t AIPL1 = 1. Where indicated the HSP90 inhibitors HSP990 (Novartis), Geldanamycin (Selleckchem) and 17-AAG (Selleckchem) were added to the cells at a concentration of 1 μM for 18 h.

PDE6 activity assay

Twenty-four hours post-transfection, cells were lysed in 0.1 N HCl. Intracellular cGMP concentration was measured using the competitive cGMP ELISA Kit (Cayman Chemical) following the manufacturer's protocols and specifications. The lysates were acetylated to detect lower concentrations of cGMP. The assay was done in triplicate and repeated at least three times.

Statistical analysis

Statistical analyses to determine p values for intergroup comparisons were conducted using the unpaired Student t-test. $p > 0.01$ was considered not significant (NS).

Supplementary Material

Supplementary Material is available at *HMG* online.

Conflict of Interest statement. None declared.

Funding

Moorfields Eye Hospital Special Trustees (ST 1307C); the Rosetrees Trust (M326); Fight for Sight/Retinitis Pigmentosa Fighting Blindness (24RP14); Retinitis Pigmentosa Fighting Blindness (GR587); and the Velux Foundation (projects 855 and 1029). The funders had no role in the study design, data collection and analysis, decision to publish or preparation of the article. Funding to pay the Open Access publication charges for this article was provided by Retinitis Pigmentosa Fighting Blindness.

References

1. Koenekoop, R.K. (2004) An overview of Leber congenital amaurosis: a model to understand human retinal development. *Surv. Ophthalmol.*, **49**, 379–398.
2. den Hollander, A.I., Roepman, R., Koenekoop, R.K. and Cremers, F.P. (2008) Leber congenital amaurosis: genes, proteins and disease mechanisms. *Prog. Retin. Eye Res.*, **27**, 391–419.
3. Sohocki, M.M., Bowne, S.J., Sullivan, L.S., Blackshaw, S., Cepko, C.L., Payne, A.M., Bhattacharya, S.S., Khaliq, S., Qasim Mehdi, S. and Birch, D.G. (2000) Mutations in a new photoreceptor-pineal gene on 17p cause Leber congenital amaurosis. *Nat. Gen.*, **24**, 79–83.
4. Dharmaraj, S., Leroy, B.P., Sohocki, M.M., Koenekoop, R.K., Perrault, I., Anwar, K., Khaliq, S., Devi, R.S., Birch, D.G., De Pool, E. *et al.* (2004) The phenotype of Leber congenital amaurosis in patients with AIPL1 mutations. *Arch. Ophthalmol.*, **122**, 1029–1037.
5. Weleber, R.G., Francis, P.J., Trzupek, K.M., Beattie, C. (1993–2017) Leber Congenital Amaurosis. 2004 Jul 7 [Updated 2013 May 2]. In: Pagon, R.A., Adam, M.P., Ardinger, H.H. *et al.* (eds), *GeneReviews®* [Internet].University of Washington, Seattle, WA. Available from: https://www.ncbi.nlm.nih.gov/books/NBK1298/
6. Aboshiha, J., Dubis, A.M., van der Spuy, J., Nishiguchi, K.M., Cheeseman, E.W., Ayuso, C., Ehrenberg, M., Simonelli, F., Bainbridge, J.W. and Michaelides, M. (2015) Preserved outer retina in AIPL1 Leber's congenital amaurosis: implications for gene therapy. *Ophthalmology*, **122**, 862–864.
7. van der Spuy, J., Chapple, J.P., Clark, B.J., Luthert, P.J., Sethi, C.S. and Cheetham, M.E. (2002) The Leber congenital amaurosis gene product AIPL1 is localized exclusively in rod photoreceptors of the adult human retina. *Hum. Mol. Gen.*, **11**, 823–831.
8. Bell, D.R. and Poland, A. (2000) Binding of aryl hydrocarbon receptor (AhR) to AhR-interacting protein. The role of hsp90. *J. Biol. Chem.*, **275**, 36407–36414.
9. Pirkl, F. and Buchner, J. (2001) Functional analysis of the Hsp90-associated human peptidyl prolyl cis/trans isomerases FKBP51, FKBP52 and Cyp40. *J. Mol. Biol.*, **308**, 795–806.
10. Hidalgo-de-Quintana, J., Evans, R.J., Cheetham, M.E. and van der Spuy, J. (2008) The Leber congenital amaurosis protein AIPL1 functions as part of a chaperone heterocomplex. *Invest. Ophthalmol. Vis. Sci.*, **49**, 2878–2887.
11. Lamb, J.R., Tugendreich, S. and Hieter, P. (1995) Tetratricopeptide repeat interactions: to TPR or not to TPR? *Trends Biochem. Sci.*, **20**, 257–259.
12. Allan, R.K. and Ratajczak, T. (2011) Versatile TPR domains accommodate different modes of target protein recognition and function. *Cell Stress Chaperones*, **16**, 353–367.
13. Johnson, J.L. (2012) Evolution and function of diverse Hsp90 homologs and cochaperone proteins. *Biochim. Biophys. Acta*, **1823**, 607–613.
14. Pearl, L.H. and Prodromou, C. (2006) Structure and mechanism of the Hsp90 molecular chaperone machinery. *Ann. Rev. Biochem.*, **75**, 271–294.
15. Young, J.C., Obermann, W.M. and Hartl, F.U. (1998) Specific binding of tetratricopeptide repeat proteins to the C-terminal 12-kDa domain of hsp90. *J. Biol. Chem.*, **273**, 18007–18010.
16. Russell, L.C., Whitt, S.R., Chen, M.S. and Chinkers, M. (1999) Identification of conserved residues required for the binding of a tetratricopeptide repeat domain to heat shock protein 90. *J. Biol. Chem.*, **274**, 20060–20063.
17. Scheufler, C., Brinker, A., Bourenkov, G., Pegoraro, S., Moroder, L., Bartunik, H., Hartl, F.U. and Moarefi, I. (2000) Structure of TPR domain-peptide complexes: critical elements in the

assembly of the Hsp70-Hsp90 multichaperone machine. *Cell*, **101**, 199–210.
18. Onuoha, S.C., Coulstock, E.T., Grossmann, J.G. and Jackson, S.E. (2008) Structural studies on the co-chaperone Hop and its complexes with Hsp90. *J. Mol. Biol.*, **379**, 732–744.
19. Cheung-Flynn, J., Roberts, P.J., Riggs, D.L. and Smith, D.F. (2003) C-terminal sequences outside the tetratricopeptide repeat domain of FKBP51 and FKBP52 cause differential binding to Hsp90. *J. Biol. Chem.*, **278**, 17388–17394.
20. Chadli, A., Bruinsma, E.S., Stensgard, B. and Toft, D. (2008) Analysis of Hsp90 cochaperone interactions reveals a novel mechanism for TPR protein recognition. *Biochemisty*, **47**, 2850–2857.
21. Lee, C.T., Graf, C., Mayer, F.J., Richter, S.M. and Mayer, M.P. (2012) Dynamics of the regulation of Hsp90 by the co-chaperone Sti1. *EMBO J.*, **31**, 1518–1528.
22. Schmid, A.B., Lagleder, S., Grawert, M.A., Rohl, A., Hagn, F., Wandinger, S.K., Cox, M.B., Demmer, O., Richter, K., Groll, M. *et al.* (2012) The architecture of functional modules in the Hsp90 co-chaperone Sti1/Hop. *EMBO J.*, **31**, 1506–1517.
23. Li, J., Zoldak, G., Kriehuber, T., Soroka, J., Schmid, F.X., Richter, K. and Buchner, J. (2013) Unique proline-rich domain regulates the chaperone function of AIPL1. *Biochemisty*, **52**, 2089–2096.
24. Yadav, R.P., Majumder, A., Gakhar, L. and Artemyev, N.O. (2015) Extended conformation of the proline-rich domain of human aryl hydrocaron recetor-interacting protein-like 1: implications for retina disease. *J. Neurochem.*, **135**, 165–175.
25. Liu, X., Bulgakov, O.V., Wen, X.H., Woodruff, M.L., Pawlyk, B., Yang, J., Fain, G.L., Sandberg, M.A., Makino, C.L. and Li, T. (2004) AIPL1, the protein that is defective in Leber congenital amaurosis, is essential for the biosynthesis of retinal rod cGMP phosphodiesterase. *Proc. Natl. Acad. Sci. U. S. A.*, **101**, 13903–13908.
26. Ramamurthy, V., Niemi, G.A., Reh, T.A. and Hurley, J.B. (2004) Leber congenital amaurosis linked to AIPL1: a mouse model reveals destabilization of cGMP phosphodiesterase. *Proc. Natl. Acad. Sci. U. S. A.*, **101**, 13897–13902.
27. Kolandaivelu, S., Huang, J., Hurley, J.B. and Ramamurthy, V. (2009) AIPL1, a protein associated with childhood blindness, interacts with alpha-subunit of rod phosphodiesterase (PDE6) and is essential for its proper assembly. *J. Biol. Chem.*, **284**, 30853–30861.
28. Kolandaivelu, S., Singh, R.K. and Ramamurthy, V. (2014) AIPL1, A protein linked to blindness, is essential for the stability of enzymes mediating cGMP metabolism in cone photoreceptor cells. *Hum. Mol. Genet.*, **23**, 1002–1012.
29. Kirschman, L.T., Kolandaivelu, S., Frederick, J.M., Dang, L., Goldberg, A.F., Baehr, W. and Ramamurthy, V. (2010) The Leber congenital amaurosis protein, AIPL1, is needed for the viability and functioning of cone photoreceptor cells. *Hum. Mol. Genet.*, **19**, 1076–1087.
30. Gopalakrishna, K.N., Boyd, K., Yadav, R.P. and Artemyev, N.O. (2016) Aryl hydrocarbon receptor-interacting protein-like 1 is an obligate chaperone of phosphodiesterase 6 and is assisted by the gamma-subunit of its client. *J. Biol. Chem.*, **291**, 16282–16291.
31. Ramamurthy, V., Roberts, M., van den Akker, F., Niemi, G., Reh, T.A. and Hurley, J.B. (2003) AIPL1, a protein implicated in Leber's congenital amaurosis, interacts with and aids in processing of farnesylated proteins. *Proc. Natl. Acad. Sci. U. S. A.*, **100**, 12630–12635.
32. Majumder, A., Gopalakrishna, K.N., Cheguru, P., Gakhar, L. and Artemyev, N.O. (2013) Interaction of aryl hydrocarbon receptor-interacting protein-like 1 with the farnesyl moiety. *J. Biol. Chem.*, **288**, 21320–21328.
33. Yu, L., Yadav, R.P. and Artemyev, N.O. (2017) NMR resonance assignments of the FKBP domain of human aryl hydrocarbon receptor-interacting protein-like 1 (AIPL1) in complex with a farnesyl ligand. *Biomol. NMR Assign.*, **11**, 111–115.
34. Aguila, M., Bevilacqua, D., McCulley, C., Schwarz, N., Athanasiou, D., Kanuga, N., Novoselov, S.S., Lange, C.A., Ali, R.R., Bainbridge, J.W. *et al.* (2014) Hsp90 inhibition protects against inherited retinal degeneration. *Hum. Mol. Genet.*, **23**, 2164–2175.
35. Bellingham, J., Davidson, A.E., Aboshiha, J., Simonelli, F., Bainbridge, J.W., Michaelides, M. and van der Spuy, J. (2015) Investigation of aberrant splicing induced by AIPL1 variations as a cause of Leber congenital amaurosis. *Invest. Ophthalmol. Vis. Sci.*, **56**, 7784–7793.
36. Gallon, V.A., Wilkie, S.E., Deery, E.C., Newbold, R.J., Sohocki, M.M., Bhattacharya, S.S., Hunt, D.M. and Warren, M.J. (2004) Purification, characterisation and intracellular localisation of aryl hydrocarbon interacting protein-like 1 (AIPL1) and effects of mutations associated with inherited retinal dystrophies. *Biochim. Biophys. Acta*, **1690**, 141–149.
37. Kanaya, K., Sohocki, M.M. and Kamitani, T. (2004) Abolished interaction of NUB1 with mutant AIPL1 involved in Leber congenital amaurosis. *Biochem. Biophys. Res. Commun.*, **317**, 768–773.
38. van der Spuy, J. and Cheetham, M.E. (2004) The Leber congenital amaurosis protein AIPL1 modulates the nuclear translocation of NUB1 and suppresses inclusion formation by NUB1 fragments. *J. Biol. Chem.*, **279**, 48038–48047.
39. Bett, J.S., Kanuga, N., Richet, E., Schmidtke, G., Groettrup, M., Cheetham, M.E. and van der Spuy, J. (2012) The inherited blindness protein AIPL1 regulates the ubiquitin-like FAT10 pathway. *PLoS One*, **7**, e30866.
40. Karan, S., Zhang, H., Li, S., Frederick, J.M. and Baehr, W. (2008) A model for transport of membrane-associated phototransduction polypeptides in rod and cone photoreceptor inner segments. *Vis. Res.*, **48**, 442–452.
41. Bolte, S. and Cordeliéres, F.P. (2006) A guided tour into subcellular colocalization analysis in light microscopy. *J. Microscopy*, **224**, 213–232.
42. Tsang, S.H., Woodruff, M.L., Hsu, C.W., Naumann, M.C., Cilluffo, M., Tosi, J. and Lin, C.S. (2011) Function of the asparagine 74 residue of the inhibitory gamma-subunit of retinal rod cGMP-phophodiesterase (PDE) in vivo. *Cell. Signal.*, **23**, 1584–1589.
43. Hidalgo-de-Quintana, J., Schwarz, N., Meschede, I.P., Stern-Schneider, G., Powner, M.B., Morrison, E.E., Futter, C.E., Wolfrum, U., Cheetham, M.E., van der Spuy, J. and Li, T. (2015) The Leber congenital amaurosis protein AIPL1 and EB proteins co-localize at the photoreceptor cilium. *PLoS One*, **10**, e0121440.
44. Linnert, M., Lin, Y.J., Manns, A., Haupt, K., Paschke, A.K., Fischer, G., Weiwad, M. and Lucke, C. (2013) The FKBP-type domain of the human aryl hydrocarbon receptor-interacting protein reveals an unusual Hsp90 interaction. *Biochemistry*, **52**, 2097–2107.
45. Cote, R.H. (2004) Characteristics of photoreceptor PDE (PDE6): similarities and differences to PDE5. *Int. J. Impot. Res.*, **16 (Suppl. 1)**, S28–S33.
46. Gietz, D., St Jean, A., Woods, R.A. and Schiestl, R.H. (1992) Improved method for high efficiency transformation of intact yeast cells. *Nucleic Acids Res.*, **20**, 1425.
47. Prodromou, C., Siligardi, G., O'Brien, R., Woolfson, D.N., Regan, L., Panaretou, B., Ladbury, J.E., Piper, P.W. and Pearl, L.H. (1999) Regulation of Hsp90 ATPase activity by tetratricopeptide repeat (TPE)-domain co-chaperones. *EMBO J.*, **18**, 754–762.
48. Kelley, L.A., Mezulis, S., Yates, C.M., Wass, M.N. and Sternberg, M.J.E. (2015) The Phyre2 web portal for protein modeling, prediction and analysis. *Nat. Protoc.*, **10**, 845–858.